NOAA Technical Report NOS OES 003

LONG ISLAND SOUND OCEANOGRAPHY PROJECT

SUMMARY REPORT, VOLUME 1:

APPLICATION AND DOCUMENTATION OF THE LONG ISLAND SOUND THREE-DIMENSIONAL CIRCULATION MODEL

Silver Spring, Maryland
January 1994

noaa National Oceanic and Atmospheric Administration

U.S. DEPARTMENT OF COMMERCE
National Ocean Service
Office of Ocean and Earth Sciences
Marine Analysis and Interpretation Division
Coastal and Estuarine Oceanography Branch

Office of Ocean and Earth Science
National Ocean Service
National Oceanic and Atmospheric Administration
U.S. Department of Commerce

The Office of Ocean and Earth Sciences provides for the understanding of the coastal and ocean environment through the conduct of applied research and development in geophysics; the measurement, analyses, and product development of ocean and lake water levels; the collection, analyses, product development, and dissemination of coastal and global marine data; and the synthesis and interpretation with numerical and mechanistic modeling of global marine data sets. The Office cooperates with the U.S. Navy in conducting oceanographic activities for defense and mixed defense-civil sector purposes and applications.

It plans, develops and coordinates NOAA participation in Federally conducted oceanographic programs and activities, and facilitates cooperative programs, projects and activities with the oceanographic research community. It monitors and analyzes oceanographic activities between NOAA and other organizations and agencies; identifies potential conflicts, overlaps, and opportunities for joint or cooperative efforts; and develops and maintains cooperative agreements, Memoranda of Understanding and other arrangements as appropriate to resolve issues and to ensure maximum benefits from programs of mutual interest. It develops and maintains inventories of oceanographic programs, projects, systems and activities of other organizations and agencies to provide a basis for integrating current and future programs, systems and activities to ensure maximum efficiency and effectiveness in meeting national goals and requirements. The Office conducts research and development; carries out theoretical studies, data analyses, and engineering development; and formulates and executes programs encompassing technological development and application to oceanography, geophysics, geodesy, and related fields .

For the Great Lakes, coastal estuaries, sea coast and oceans, the Office plans, develops, and applies numerical and mechanistic models and produces predictions, forecasts, and analysis guidance materials of oceanographic and related marine meteorological phenomena; collects, analyzes and disseminates tide and water-level observations and associated information; and computes water-level datums for hydrographic, marine boundary and other special surveys. It evaluates and improves methods of data analysis; compares and integrates existing and new classes of data and products; provides and quality controls data sets and an array of output products; and assures science and technology transfer to and from the Office's programs and projects. The Office produces and disseminates operational marine environmental forecast and analysis guidance materials; manages and supports ocean climate studies; installs and operates real-time marine data collection systems; and formulates requirements for marine data sets and for data processing and communications systems; and designs and manages computer-based systems in support of these requirements.

NOAA Technical Report NOS OES 003

LONG ISLAND SOUND OCEANOGRAPHY PROJECT

SUMMARY REPORT, VOLUME 1:

APPLICATION AND DOCUMENTATION OF THE LONG ISLAND SOUND THREE-DIMENSIONAL CIRCULATION MODEL

Richard A. Schmalz, Jr.

January 1994

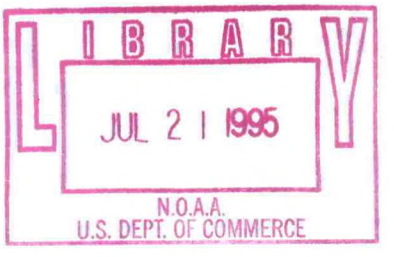

U.S. DEPARTMENT OF COMMERCE
Ronald H. Brown, Secretary

National Oceanic and Atmospheric Administration
D. James Baker, Under Secretary

National Ocean Service
W. Stanley Wilson
Assistant Administrator

Office of Ocean and Earth Sciences
Melbourne G. Briscoe

Marine Analysis and Interpretation Division
Ledolph Baer

Coastal and Estuarine Oceanography Branch
Bruce Parker

NOTICE

Mention of a commercial company or product does not constitute an endorsement by NOAA. Use for publicity or advertising purposes of information from the publication concerning proprietary products or the tests of such products is not authorized.

TABLE OF CONTENTS

LIST OF FIGURES

LIST OF TABLES

ABSTRACT

Using extensive physical oceanographic measurements, the National Oceanic and Atmospheric Administration's (NOAA) National Ocean Service (NOS) has developed a three-dimensional hydrodynamic model of Long Island Sound to provide residual circulation information for use in Environmental Protection Agency (EPA) water quality modeling and management studies. The hydrodynamic model was also utilized to develop an atlas of astronomic tide and density driven currents and water levels.

The Blumberg-Mellor (1980,1987) three-dimensional hydrodynamic model used in this study was supplied to NOAA-NOS in September 1989 by Professor George L. Mellor of Princeton University, along with an initial version of documentation (Mellor, 1989). That model, although adapted to Long Island Sound, initially contained generalized initial and boundary forcings. This report describes the model and the model enhancements required to provide freshwater inflows, initial conditions, and boundary forcings in the NOS application to Long Island Sound. The hydrodynamic model uses a rectilinear horizontal grid with 2-km cell size and seven vertical levels (repesenting a compromise between spatial resolution and computational efficiency) in application to Long Island Sound. The model, as presently configured, is able to describe realistic, observationally-consistent residual and tidal circulations at hourly time and order 2 km space scales, respectively.

This report documents the full set of model equations, their approximation via finite differences, and numerical solution techniques. Present model enhancements, including restart mechanics, residual circulation, freshwater inflow specification, and tidal statistics are discussed prior to considering the specifics of the model application to Long Island Sound. The model application is presented in terms of grid development and associated stability conditions, initial and boundary condition specification, and computational requirements. Possible future model enchancements are also considered.

1. INTRODUCTION

The National Oceanic and Atmospheric Administration's (NOAA) National Ocean Service (NOS) has conducted extensive physical oceanographic measurements and developed a three-dimensional hydrodynamic model to provide residual circulation data to drive a companion water quality model in support of the Long Island Sound Study (LISS). LISS is a major intergovernmental program involving several NOAA components working in collaboration with the states of New York and Connecticut and the Environmental Protection Agency (EPA) in order to develop a master environmental plan to address hypoxic or anoxic conditions and safeguard the general water quality of the Sound. The master plan will be based in substantial part on coupled NOAA hydrodynamic model and EPA-sponsored water quality model simulations over the eighteen month period of April 1988 - September 1989.

The Coastal and Estuarine Oceanography Branch (CEOB) in the Office of Ocean and Earth Sciences (OES) has collected data (Earwaker et al., 1990) to complement EPA's physical oceanographic measurement program and to verify the Long Island Sound hydrodynamic model. An important additional use of the data is to revise NOS tide and current predictions in Long Island Sound.

The documentation and application to Long Island Sound of the NOS three-dimensional hydrodynamic model is the subject of this report (Volume 1 of the series). In Volume 2, residual and thermohaline circulation is discussed and related to the current and previous observations and the results of an eighteen month simulation over the period of April 1988 - September 1989. Volume 3 contains copies of scientific papers published elsewhere, primarily in peer-reviewed journals.

The three-dimensional hydrodynamic model employed in NOS's Long Island Sound Oceanography Project was developed by Professor George L. Mellor of Princeton University and Dr. Alan F. Blumberg of HydroQual, Inc., (1980,1987) under support of NOAA's Geophysical Fluid Dynamics Laboratory, Sea Grant Office, and National Ocean Service and the U.S. Navy's Office of Naval Research and Institute of Naval Oceanography. The model employs a primitive equation approach implemented using finite differences. The principal attributes of the model are the following:

1) imbedded second-moment turbulence closure sub-model,
2) sigma stretching of the vertical coordinate,
3) horizontal space-staggered grid,
4) explicit in the horizontal, implicit in the vertical,
5) free surface,
6) split (external- and internal-) mode concept, and
7) realistic thermodynamics.

CEOB has previously applied the model in a two-dimensional (external) mode in a real-time

operational model/measurement system for Delaware River and Bay (Patchen, 1986). The model in three dimensions (external- and internal-mode) has been successfully applied to the Hudson-Raritan estuary (Oey et al. 1985a,b,c), to Chesapeake Bay (Blumberg and Goodrich, 1990), and to the New York Bight (Blumberg and Galperin, 1990). As a result of CEOB's previous successful application in Delaware River and Bay, this model was selected for application to Long Island Sound. The hydrodynamic model was given to NOS in September 1989 by Professor Mellor along with an initial version of documentation (Mellor, 1989). The model as supplied was adapted to Long Island Sound from the Gulf Stream version and contained generalized estuarine initial and boundary forcings.

Prior to detailed application to Long Island Sound, the supporting model papers [Blumberg-Mellor (1980,1987), Mellor (1989)] were reviewed and the main features are documented in Section 2 on the basic model formulation. The governing hydrodynamic equations are presented initially in Cartesian coordinates and then transformed to a vertical sigma coordinate to form the internal-mode model component. These transformed equations are further vertically integrated to obtain the external-mode model component. Finite difference approximations are then presented in operator form and the numerical solution techniques briefly outlined. In Section 3, model enhancements for realistic application to the Sound in terms of restart, residual circulation, freshwater inflows, and tidal statistical techniques are presented. In Section 4, the model application to Long Island Sound is discussed first in terms of the development of the computational grid. Initial condition procedures, and boundary conditions for both internal- and external- mode components are next presented. Long term computational requirements necessary for simulation of eighteen month residual circulation are next considered. Possible future model enhancements are advanced in Section 5, while report results are summarized and conclusions drawn in Section 6.

2. MODEL FORMULATION

In this section the governing three-dimensional hydrodynamic equations in Cartesian coordinates are developed and then transformed to a vertically-stretched sigma terrain-following coordinate. Two equation sets are developed (one for the external- and one for the internal-mode equations). Finite difference approximations are then presented for the vertical velocity and both computational mode equation sets. Finally, numerical solution techniques and stability requirements are discussed.

2.1. Governing Hydrodynamic Equations

The partial differential equation set is presented initially in terms of Cartesian coordinates. The equation of state is discussed separately, since it is independent of coordinates. The vertical sigma coordinate transformation is next developed for both the internal and external mode formulations.

Cartesian Coordinate Equation Set

Blumberg and Mellor (1987) have described a three-dimensional coastal ocean circulation model assuming hydrostatic pressure and Boussinesq approximations as given in the following equations

$$\frac{\partial u}{\partial x} + \frac{\partial v}{\partial y} + \frac{\partial w}{\partial z} = 0 \qquad (2.1)$$

(Continuity)

$$\frac{\partial u}{\partial t} + u\frac{\partial u}{\partial x} + v\frac{\partial u}{\partial y} + w\frac{\partial u}{\partial z} - fv + \frac{1}{\rho_o}\frac{\partial P}{\partial x} = \frac{\partial}{\partial x}\left[2A_M\frac{\partial u}{\partial x}\right] + \frac{\partial}{\partial y}\left[A_M\left(\frac{\partial u}{\partial y} + \frac{\partial v}{\partial x}\right)\right] + \frac{\partial}{\partial z}\left[K_m\frac{\partial u}{\partial z}\right] \qquad (2.2)$$

(x-momentum)

$$\frac{\partial v}{\partial t} + u\frac{\partial v}{\partial x} + v\frac{\partial v}{\partial y} + w\frac{\partial v}{\partial z} + fu + \frac{1}{\rho_o}\frac{\partial P}{\partial y} = \frac{\partial}{\partial y}\left[2A_M\frac{\partial v}{\partial y}\right] + \frac{\partial}{\partial x}\left[A_M\left(\frac{\partial u}{\partial y} + \frac{\partial v}{\partial x}\right)\right] + \frac{\partial}{\partial z}\left[K_m\frac{\partial v}{\partial z}\right] \qquad (2.3)$$

(y-momentum)

$$\frac{\partial P}{\partial z} = -\rho g \qquad (2.4)$$

(z-momentum)

$$\frac{\partial T}{\partial t} + u\frac{\partial T}{\partial x} + v\frac{\partial T}{\partial y} + w\frac{\partial T}{\partial z} = \frac{\partial}{\partial x}\left[A_H\frac{\partial T}{\partial x}\right] + \frac{\partial}{\partial y}\left[A_H\frac{\partial T}{\partial y}\right] + \frac{\partial}{\partial z}\left[K_H\frac{\partial T}{\partial z}\right] \quad \text{(Temperature)} \tag{2.5}$$

$$\frac{\partial S}{\partial t} + u\frac{\partial S}{\partial x} + v\frac{\partial S}{\partial y} + w\frac{\partial S}{\partial z} = \frac{\partial}{\partial x}\left[A_H\frac{\partial S}{\partial x}\right] + \frac{\partial}{\partial y}\left[A_H\frac{\partial S}{\partial y}\right] + \frac{\partial}{\partial z}\left[K_H\frac{\partial S}{\partial z}\right] \quad \text{(Salinity)} \tag{2.6}$$

where

(x,y,z) ≡ east, north, and vertical coordinates, respectively,
(u,v,w) ≡ velocity components in x,y, and z directions, respectively,
t ≡ time,
f ≡ Coriolis parameter,
ρ ≡ water density,
ρ_o ≡ reference water density,
P ≡ pressure,
g ≡ gravitational acceleration,
T ≡ temperature,
S ≡ salinity,
A_M ≡ horizontal momemtum mixing coefficient,
K_m ≡ vertical momemtum mixing coefficient,
A_H ≡ horizontal constituent mixing coefficient, and
K_H ≡ vertical constituent (salinity or temperature) mixing coefficient.

The Mellor and Yamada (1982) turbulence closure scheme is used to determine the vertical mixing coefficients, K_m and K_H. The closure equations for turbulent kinetic energy (T. K. E.), q^2, and turbulent macroscale, ℓ, are given by

$$\frac{\partial(q^2)}{\partial t} + u\frac{\partial(q^2)}{\partial x} + v\frac{\partial(q^2)}{\partial y} + w\frac{\partial(q^2)}{\partial z} = 2K_m\left[\left(\frac{\partial u}{\partial z}\right)^2 + \left(\frac{\partial v}{\partial z}\right)^2\right] \tag{2.7}$$
$$+ \frac{2g}{\rho_o}K_H\frac{\partial \rho}{\partial z} - \frac{2q^3}{B_1\ell} + \frac{\partial}{\partial x}\left[A_H\frac{\partial(q^2)}{\partial x}\right] + \frac{\partial}{\partial y}\left[A_H\frac{\partial(q^2)}{\partial y}\right] + \frac{\partial}{\partial z}\left[K_q\frac{\partial(q^2)}{\partial z}\right] \quad \text{(T. K. E.)}$$

$$\frac{\partial(q^2\ell)}{\partial t} + u\frac{\partial(q^2\ell)}{\partial x} + v\frac{\partial(q^2\ell)}{\partial y} + w\frac{\partial(q^2\ell)}{\partial z} = \ell E_1 K_m\left[\left(\frac{\partial u}{\partial z}\right)^2 + \left(\frac{\partial v}{\partial z}\right)^2\right] \tag{2.8}$$
$$+ \frac{\ell E_1 g}{\rho_o}K_H\frac{\partial \rho}{\partial z} - \frac{q^3}{B_1}\varpi + \frac{\partial}{\partial x}\left[A_H\frac{\partial(q^2\ell)}{\partial x}\right] + \frac{\partial}{\partial y}\left[A_H\frac{\partial(q^2\ell)}{\partial y}\right] + \frac{\partial}{\partial z}\left[K_q\frac{\partial(q^2\ell)}{\partial z}\right] \quad \text{(Turbulent macroscale)}$$

The wall function is ϖ. Near surfaces, $\varpi = 1 + E_2$, while away from surfaces, $\varpi = 1$. The

vertical mixing coefficients K_m, K_H, and K_q are given by the following

$$\begin{aligned} K_m &= \ell q S_M \\ K_H &= \ell q S_H \\ K_q &= \ell q S_q \end{aligned} \qquad (2.9)$$

(Vertical Mixing Coefficients)

where S_M, S_H, and, S_q are analytically-derived stability functions, which we now develop. Defining,

$$\begin{aligned} G_m &= \frac{\ell^2}{q^2}\left[\left(\frac{\partial u}{\partial z}\right)^2 + \left(\frac{\partial v}{\partial z}\right)^2\right] \\ G_H &= \frac{\ell^2}{q^2}\frac{g}{\rho_o}\frac{\partial \rho}{\partial z}\ , \end{aligned} \qquad (2.10)$$

then the stability functions are given as outlined in Galperin et al. (1988) by

$$\begin{aligned} &S_H(1 - 3A_2 B_2 G_H - 18A_1 A_2 G_H) = A_2(1 - 6A_1/B_1) \\ &S_M(1 - 9A_1 A_2 G_H) - S_H(18A_1^2 G_H + 9A_1 A_2 G_H) = A_1(1 - 3C_1 - 6A_1/B_1)\ . \end{aligned} \qquad (2.11)$$

(Mixing Equation Set)

Based on laboratory data, Blumberg and Mellor (1987) specify the constants in Equations (2.7)-(2.11) as

$$\begin{aligned} (A_1, A_2, B_1, B_2, C_1) &= (0.92, 0.74, 16.6, 10.1, 0.08) \\ (E_1, E_2) &= (1.8, 1.33)\ . \end{aligned} \qquad (2.12)$$

(Experimental constants)

For horizontal diffusivity, the approach suggested by Smagorinsky (1963) is used to specify A_M in terms of the deformation field defined on the computational grid (Δx, Δy) as given by

$$A_M = k_H^2 (\Delta x \Delta y)\left[\left(\frac{\partial u}{\partial x} - \frac{\partial v}{\partial y}\right)^2 + \left(\frac{\partial v}{\partial x} + \frac{\partial u}{\partial y}\right)^2\right]^{0.5}\ . \qquad (2.13)$$

In this study, A_M is considered equal to A_H. Smagorinsky (1963) used $k_H \approx 0.08$. In a simulation of the planetary boundary layer Chow (1971) specified $k_H = \frac{\kappa}{\sqrt{2}} = 0.29$, where $\kappa = .41$ is von Karman's constant. In the present study k_H is set to 0.22 in the East River and throughout Long Island and Block Island Sounds, and is set to 0.5 in the five rivers in Connecticut and in the Harlem River to represent intense lateral mixing processes.

Equation of State

The following relationship for density reported by Knudsen (1901) and consistent with measurements of specific gravity by Forsch et al. (1902) is employed. Density is expressed in terms of σ_t as follows

$$\sigma_t = \left[\frac{\rho}{\rho_m} - 1 \right] 10^3 \tag{2.14}$$

where $\sigma_t \equiv$ sigma t and
$\rho_m \equiv$ density of distilled water at 4 °C (999.975 kg/m^3).

Then σ_t is expressed as a function of salinity, S, and temperature, T as given by

$$\sigma_t = \Sigma_t + (\sigma_o - \Sigma_o)\left[1 - A_t + B_t(\sigma_o + \Sigma_o)\right] \tag{2.15}$$

where

$$\Sigma_t = -(T - 3.98)^2 \frac{(T + 283)}{503.570\,(T + 67.26)} ,$$

$$\Sigma_o = -0.1324 ,$$

$$\sigma_o = -.093445862 + .814876576S - .00048249614S^2 + .676786135 \times 10^{-6}S^3 ,$$

$$A_t = 4.7867 \times 10^{-3}T - 9.8185 \times 10^{-5}T^2 + 1.0843 \times 10^{-6}T^3 , \text{ and}$$

$$B_t = 1.8030 \times 10^{-5}T - 8.164 \times 10^{-7}T^2 + 1.667 \times 10^{-8}T^3 .$$

Sigma Coordinate Equation Set

The vertical coordinate, z in Equations (2.1) - (2.8), is transformed using the so-called σ stretching. Consider the hydrodynamic variable $F(x,y,z,t)$ expressed in a standard right-handed Cartesian system. Let us examine how derivatives of F may be expressed in an alternate vertically stretched system defined in the following manner.

$$x' = x \tag{2.16a}$$

$$y' = y \tag{2.16b}$$

$$\sigma = \frac{z - \eta}{H} \tag{2.16c}$$

$$t' = t \tag{2.16d}$$

where

(x', y', σ, t') ≡ transformed spatial coordinates and time,
η ≡ water surface elevation above model datum,
h ≡ water depth with respect to model datum, and
H ≡ total water depth $(\eta + h)$.

First consider the partial derivative, $\frac{\partial F}{\partial x}$. By the Chain Rule for partial differentiation, obtain

$$\frac{\partial F}{\partial x} = \frac{\partial F}{\partial x'} + \frac{\partial F}{\partial \sigma}\frac{\partial \sigma}{\partial x'} = \frac{\partial F}{\partial x'} - \frac{\partial F}{\partial \sigma}\left[\frac{1}{H}\frac{\partial \eta}{\partial x'} + \frac{\sigma}{H}\frac{\partial H}{\partial x'}\right] . \tag{2.17}$$

Note that $\frac{\partial \sigma}{\partial x} = -\frac{1}{H}\left[\frac{\partial \eta}{\partial x} + \sigma\frac{\partial H}{\partial x}\right]$ and also, $\frac{\partial \eta}{\partial x} = \frac{\partial \eta}{\partial x'}$ and $\frac{\partial H}{\partial x} = \frac{\partial H}{\partial x'}$ because η and H *are not functions of* σ.

By analogous arguments, one obtains a similar expression for $\frac{\partial F}{\partial y}$.

Next observe that

$$\frac{\partial F}{\partial z} = \frac{1}{H}\frac{\partial F}{\partial \sigma} . \tag{2.18}$$

Also

$$\frac{\partial F}{\partial t} = \frac{\partial F}{\partial t'}\frac{\partial t'}{\partial t} + \frac{\partial F}{\partial \sigma}\frac{\partial \sigma}{\partial t} = \frac{\partial F}{\partial t'} + \frac{\partial F}{\partial \sigma}\left[-\frac{1}{H}\frac{\partial \eta}{\partial t} - \frac{\sigma}{H}\frac{\partial H}{\partial t}\right] . \tag{2.19}$$

Next consider the vertical velocity component,

$$w = \frac{dz}{dt} = \frac{d}{dt}(\sigma H + \eta) = H\frac{d\sigma}{dt} + \sigma\frac{dH}{dt} + \frac{d\eta}{dt} \quad . \tag{2.20}$$

Observe that η and H are not functions of z, $\frac{dx}{dt} = u = \frac{dx'}{dt}$, and $\frac{dy}{dt} = v = \frac{dy'}{dt}$.

Defining $\omega = H\frac{d\sigma}{dt}$ and $\frac{d(\,)}{dt} = \frac{\partial(\,)}{\partial t} + u\frac{\partial(\,)}{\partial x} + v\frac{\partial(\,)}{\partial y} + w\frac{\partial(\,)}{\partial z}$,

then Equation (2.20) may be written as

$$w = \omega + u\left[\sigma\frac{\partial H}{\partial x'} + \frac{\partial \eta}{\partial x'}\right] + v\left[\sigma\frac{\partial H}{\partial y'} + \frac{\partial \eta}{\partial y'}\right] + \left[\sigma\frac{\partial H}{\partial t} + \frac{\partial \eta}{\partial t}\right] \quad . \tag{2.21}$$

First consider Equation (2.1), the continuity equation. Obtain the following forms for each of the three derivatives in turn below.

$$H\frac{\partial u}{\partial x} = H\frac{\partial u}{\partial x'} - \left[\left(\frac{\partial \eta}{\partial x'} + \sigma\frac{\partial H}{\partial x'}\right)\frac{\partial u}{\partial \sigma}\right] \tag{2.22a}$$

$$H\frac{\partial v}{\partial y} = H\frac{\partial v}{\partial y'} - \left[\left(\frac{\partial \eta}{\partial y'} + \sigma\frac{\partial H}{\partial y'}\right)\frac{\partial v}{\partial \sigma}\right] \tag{2.22b}$$

$$H\frac{\partial w}{\partial z} = \frac{\partial w}{\partial \sigma} = \frac{\partial \omega}{\partial \sigma} + u\frac{\partial H}{\partial x'} + v\frac{\partial H}{\partial y'} + \frac{\partial H}{\partial t} + \frac{\partial u}{\partial \sigma}\left[\frac{\partial \eta}{\partial x'} + \sigma\frac{\partial H}{\partial x'}\right] + \frac{\partial v}{\partial \sigma}\left[\frac{\partial \eta}{\partial y'} + \sigma\frac{\partial H}{\partial y'}\right] \quad . \tag{2.22c}$$

Assembling all results, obtain

$$\frac{\partial \eta}{\partial t} + \frac{\partial Hu}{\partial x'} + \frac{\partial Hv}{\partial y'} + \frac{\partial \omega}{\partial \sigma} = 0 \quad . \tag{2.23}$$

The vertical velocity is computed from continuity in the following manner. Initially, the continuity equation (Equation (I.1) in Table 2.1) is integrated from the free surface (σ=0) to an arbitrary level σ to obtain

$$\int_0^\sigma \frac{\partial \eta}{\partial t}d\sigma + \int_0^\sigma \frac{\partial (Hu)}{\partial x'}d\sigma + \int_0^\sigma \frac{\partial (Hv)}{\partial y'}d\sigma + \int_0^\sigma \frac{\partial \omega}{\partial \sigma}d\sigma = 0 \quad . \tag{2.24}$$

Apply the boundary condition $\omega\,(0) = 0$ to obtain

$$\sigma\frac{\partial\eta}{\partial t} + \int_0^\sigma \left[\frac{\partial(Hu)}{\partial x'} + \frac{\partial(Hv)}{\partial y'}\right] d\sigma + \omega\,(\sigma) = 0 \quad . \tag{2.25}$$

The above relationship is then solved for $\omega(\sigma)$.

Next, consider the total derivative term on the left-hand side of the x momentum equation; e.g.,

$$\frac{\partial u}{\partial t} + \frac{\partial uu}{\partial x} + \frac{\partial uv}{\partial y} + \frac{\partial uw}{\partial z}. \tag{2.26}$$

Note the following relations.

$$\frac{\partial u}{\partial t} = \frac{\partial u}{\partial t} + \frac{\partial u}{\partial\sigma}\frac{\partial\sigma}{\partial t} = \frac{\partial u}{\partial t} - \left[\frac{1}{H}\frac{\partial\eta}{\partial t} + \frac{\sigma}{H}\frac{\partial H}{\partial t}\right]\frac{\partial u}{\partial\sigma} \tag{2.27a}$$

$$\frac{\partial uu}{\partial x} = 2u\frac{\partial u}{\partial x} = 2u\left[\frac{\partial u}{\partial x'} - \left[\frac{1}{H}\frac{\partial\eta}{\partial x} + \frac{\sigma}{H}\frac{\partial H}{\partial x}\right]\frac{\partial u}{\partial\sigma}\right] \tag{2.27b}$$

$$\frac{\partial uv}{\partial y} = u\frac{\partial v}{\partial y} + v\frac{\partial u}{\partial y} = u\left[\frac{\partial v}{\partial y'} - \left[\frac{1}{H}\frac{\partial\eta}{\partial y'} + \frac{\sigma}{H}\frac{\partial H}{\partial y'}\right]\frac{\partial v}{\partial\sigma}\right] \tag{2.27c}$$

$$+ v\left[\frac{\partial u}{\partial y'} - \left[\frac{1}{H}\frac{\partial\eta}{\partial y'} + \frac{\sigma}{H}\frac{\partial H}{\partial y'}\right]\frac{\partial u}{\partial\sigma}\right]$$

$$\frac{\partial uw}{\partial y} = u\frac{\partial w}{\partial y} + w\frac{\partial u}{\partial y} = \frac{u}{H}\left\{\frac{\partial\omega}{\partial\sigma} + u\frac{\partial H}{\partial x'} + v\frac{\partial H}{\partial y'} + \frac{\partial H}{\partial t}\right. \tag{2.27d}$$

$$\left. + \sigma\frac{\partial u}{\partial\sigma}\frac{\partial H}{\partial x'} + \sigma\frac{\partial v}{\partial\sigma}\frac{\partial H}{\partial y'} + \frac{\partial u}{\partial\sigma}\frac{\partial\eta}{\partial x'} + \frac{\partial v}{\partial\sigma}\frac{\partial\eta}{\partial y'}\right\}$$

$$+ \frac{1}{H}\frac{\partial u}{\partial\sigma}\left[\omega + u\left[\sigma\frac{\partial H}{\partial x'} + \frac{\partial\eta}{\partial x'}\right] + v\left[\sigma\frac{\partial H}{\partial y'} + \frac{\partial\eta}{\partial y'}\right] + \left[\sigma\frac{\partial H}{\partial t} + \frac{\partial\eta}{\partial t}\right]\right] \quad .$$

Assembling results, we finally obtain

$$\frac{D(u)}{Dt} = \frac{\partial u}{\partial t} + \frac{\partial uu}{\partial x} + \frac{\partial uv}{\partial y} + \frac{\partial uw}{\partial z} = \frac{1}{H}\left[\frac{\partial Hu}{\partial t} + \frac{\partial Hu^2}{\partial x'} + \frac{\partial Huv}{\partial y'} + \frac{\partial\omega u}{\partial\sigma}\right] \cdot \tag{2.28}$$

In order to obtain relations for the total and material derivative terms on the left-hand side of the y motion equation, the temperature equation, and the salinity equation, one substitutes v, T, and S for u appropriately to obtain:

$$\frac{D(v)}{Dt} = \frac{1}{H}\left[\frac{\partial Hv}{\partial t} + \frac{\partial Huv}{\partial x'} + \frac{\partial Hv^2}{\partial y'} + \frac{\partial \omega v}{\partial \sigma}\right] \tag{2.29a}$$

$$\frac{D(T)}{Dt} = \frac{1}{H}\left[\frac{\partial HT}{\partial t} + \frac{\partial HuT}{\partial x'} + \frac{\partial HvT}{\partial y'} + \frac{\partial \omega T}{\partial \sigma}\right] \tag{2.29b}$$

$$\frac{D(S)}{Dt} = \frac{1}{H}\left[\frac{\partial HS}{\partial t} + \frac{\partial HuS}{\partial x'} + \frac{\partial HvS}{\partial y'} + \frac{\partial \omega S}{\partial \sigma}\right] . \tag{2.29c}$$

Similar relations hold for the left-hand sides of the two turbulence equations.

Next use the vertical momentum equation to evaluate the horizontal pressure gradient terms on the left-hand side of the two horizontal momentum equations. Consider $\frac{\partial P}{\partial z} = -\rho g$, where the hydrostatic assumption is invoked for the z momentum equation. Perform the coordinate transformation to obtain

$$x = x', \quad y = y', \quad z = \sigma H + \eta$$

$$\frac{\partial P}{\partial z} = \frac{\partial P}{H \partial \sigma} = -\rho g \quad \Rightarrow \quad \frac{\partial P}{\partial \sigma} = -\rho g H \ . \tag{2.30}$$

If one integrates from σ to the free surface, then

$$\int_{\sigma}^{0} \frac{\partial P}{\partial \sigma} d\sigma = \int_{\sigma}^{0} -\rho g H \, d\sigma \quad \text{and} \tag{2.31a}$$

$$P(0) - P(\sigma) = -gH\int_{\sigma}^{0} \rho \, d\sigma \quad \Rightarrow \quad P(\sigma) = P(0) + gH\int_{\sigma}^{0} \rho \, d\sigma \ . \tag{2.31b}$$

From previous work,

$$\frac{\partial P}{\partial x} = \frac{\partial P}{\partial x'} - \left[\frac{1}{H}\frac{\partial \eta}{\partial x'} + \frac{\sigma}{H}\frac{\partial H}{\partial x'}\right]\frac{\partial P}{\partial \sigma}. \tag{2.32}$$

Evaluate $\frac{\partial P}{\partial x'}$ as follows

$$\frac{\partial P}{\partial x'} = \frac{\partial P(0)}{\partial x'} + \frac{\partial}{\partial x'}\left[gH\int_{\sigma}^{0}\rho\, d\sigma\right] = \frac{\partial P(0)}{\partial x'} + g\frac{\partial H}{\partial x'}\int_{\sigma}^{0}\rho\, d\sigma + gH\frac{\partial}{\partial x'}\left[\int_{\sigma}^{0}\rho\, d\sigma\right] .$$

Collecting all results, one obtains

$$\frac{\partial P}{\partial x} = \frac{\partial P(0)}{\partial x'} + g\frac{\partial H}{\partial x'}\int_{\sigma}^{0}\rho\, d\sigma + gH\frac{\partial}{\partial x'}\left[\int_{\sigma}^{0}\rho\, d\sigma\right] + \rho g\left[\frac{\partial \eta}{\partial x'} + \sigma\frac{\partial H}{\partial x'}\right] \qquad (2.33)$$

In an attempt to further simplify this equation, perform an integration by parts on the second term on the right-hand side to obtain

$$\frac{\partial P}{\partial x} = \frac{\partial P\,(0)}{\partial x'} + g\frac{\partial H}{\partial x'}\left[-\sigma\rho - \int_{\sigma}^{0}\sigma\frac{\partial \rho}{\partial \sigma}\, d\sigma\right] + gH\frac{\partial}{\partial x'}\left[\int_{\sigma}^{0}\rho d\sigma\right] + \rho g\left[\frac{\partial \eta}{\partial x'} + \sigma\frac{\partial H}{\partial x'}\right] .$$

Further simplify and set $P_a = P(0)$ to obtain

$$\frac{\partial P}{\partial x} = \frac{\partial P_a}{\partial x'} - g\frac{\partial H}{\partial x'}\int_{\sigma}^{0}\sigma\frac{\partial \rho}{\partial \sigma}\, d\sigma + gH\frac{\partial}{\partial x'}\left[\int_{\sigma}^{0}\rho d\sigma\right] + \rho g\frac{\partial \eta}{\partial x'} . \qquad (2.34)$$

Similarly, one may obtain

$$\frac{\partial P}{\partial y} = \frac{\partial P_a}{\partial y'} - g\frac{\partial H}{\partial y'}\int_{\sigma}^{0}\sigma\frac{\partial \rho}{\partial \sigma}\, d\sigma + gH\frac{\partial}{\partial y'}\left[\int_{\sigma}^{0}\rho d\sigma\right] + \rho g\frac{\partial \eta}{\partial y'} . \qquad (2.35)$$

The Coriolis terms on the left-hand sides of the x and y momentum equations, become

$$fu(x, y, z, t) = fu(x', y', \sigma, t) \qquad (2.36a)$$

$$fv(x, y, z, t) = fv(x', y', \sigma, t) . \qquad (2.36b)$$

The horizontal diffusion terms appearing on the right-hand sides of the x and y momentum equations (Equation (2.2) and Equation (2.3)) and constituent equations (Equation (2.5) - Equation (2.8)) are much more complex. Consider the following type term

$$HF_{x_i x_i} = H\frac{\partial}{\partial x_i}\left[A\frac{\partial \theta}{\partial x_i}\right] \qquad (2.37)$$

where x_i, $i = 1, 2 = x, y$ and $\theta = \{u, v, T, S, q^2, q^2\ell\}$.

It may be shown by expanding the right hand side that

$$H\frac{\partial}{\partial x_i}\left[A\frac{\partial \theta}{\partial x_i}\right] = \frac{\partial}{\partial x'_i}\left[AH\frac{\partial \theta}{\partial x_i}\right] + \frac{\partial}{\partial \sigma}\left[\frac{\partial \sigma}{\partial x_i}AH\frac{\partial \theta}{\partial x_i}\right] \quad . \tag{2.38}$$

In this form, the original partial differentiation with respect to x_i is replaced by a partial derivative with respect to x'_i and σ, with H being included in the partial derivatives.

Next it may be shown, by expansion of the right hand side, that the key term, $AH\frac{\partial \theta}{\partial x_i}$, inside each of these two partial derivatives can be represented as follows

$$AH\frac{\partial \theta}{\partial x_i} = A\frac{\partial (H\theta)}{\partial x'_i} + A\frac{\partial}{\partial \sigma}\left[H\frac{\partial \sigma}{\partial x_i}\theta\right] \quad . \tag{2.39}$$

Note similarly that the partial differentiation with respect to x_i is replaced by a partial derivative with respect to x'_i and σ, with again H being incorporated in the partial derivatives.

This approach allows the horizontal diffusion terms in the momemtum and constitutent equations to be written in a compact form. All vertical partial derivatives may be readily transformed by noting $\partial ( ) / \partial z = H^{-1} \partial ( ) / \partial \sigma$. Additional terms in the turbulent kinetic energy and macroscale equations are evaluated in the transformed coordinate system. The complete internal-mode sigma-stretched hydrodynamic equation set is compiled in Table 2.1 with supplemental relations given in Table 2.2.

Mellor and Blumberg (1985) argue that if horizontal and vertical resolution are sufficiently small, the horizontal diffusion terms may be neglected. In essence, diffusion is explicitly taken into account by resolved small-scale horizontal advection followed by vertical mixing. In the application to Long Island Sound, horizontal and vertical resolution are insufficent to follow this approach. Horizontal diffusion terms are included in the modified form suggested by Mellor and Blumberg (1985). They argue that a simple way to obtain a formulation consistent at the bottom when $A_m \gg K_m$, is to consider $\partial\sigma/\partial x = \partial\sigma/\partial y = 0$ (Equation (S.1) in Table 2.2) in the horizontal diffusion terms in Table 2.1 only. A consistent bottom formulation is one in which the bottom stresses, $\tau_{\sigma x}$ and $\tau_{\sigma y}$, do not contain terms of A_m. This approach is adopted in the momemtum equations and is also used for horizontal diffusion in the temperature, salinity, turbulent kinetic energy, and turbulent macroscale equations. One problem with this approach is that if there is no initial motion and temperature, salinity, and hence density are functions of z with constant horizontal diffusivities, a cross-slope baroclinically driven flow will result. In the present study, the velocity gradient dependent Smagorinsky (1963) formulation has been utilized to minimize this problem.

Table 2.1. Internal-Mode Sigma Stretched Hydrodynamic Equations

(I.1) Continuity

$$\frac{\partial \eta}{\partial t} + \frac{\partial (Hu)}{\partial x'} + \frac{\partial (Hv)}{\partial y'} + \frac{\partial \omega}{\partial \sigma} = 0$$

(I.2) x'-Momentum

$$\begin{aligned}\frac{\partial (Hu)}{\partial t} + \frac{\partial (Hu^2)}{\partial x'} + \frac{\partial (Huv)}{\partial y'} + \frac{\partial (\omega u)}{\partial \sigma} &= fHv - \frac{\rho g H}{\rho_o}\frac{\partial \eta}{\partial x'} - \frac{H}{\rho_o}\frac{\partial P_a}{\partial x'} \\ &+ \frac{gH}{\rho_o}\frac{\partial H}{\partial x'}\int_\sigma^0 \sigma \frac{\partial \rho}{\partial \sigma} d\sigma - \frac{gH^2}{\rho_o}\frac{\partial}{\partial x'}\left[\int_\sigma^0 \rho d\sigma\right] + \frac{\partial \tau_{x'x'}}{\partial x'} + \frac{\partial}{\partial \sigma}\left[\frac{\partial \sigma}{\partial x}\tau_{x'x'}\right] \\ &+ \frac{\partial \tau_{y'x'}}{\partial y'} + \frac{\partial}{\partial \sigma}\left[\frac{\partial \sigma}{\partial y}\tau_{y'x'}\right] + H^{-1}\frac{\partial}{\partial \sigma}\left[K_m \frac{\partial u}{\partial \sigma}\right]\end{aligned}$$

(I.3) y'-Momentum

$$\begin{aligned}\frac{\partial (Hv)}{\partial t} + \frac{\partial (Hvu)}{\partial x'} + \frac{\partial (Hv^2)}{\partial y'} + \frac{\partial (\omega v)}{\partial \sigma} &= -fHu - \frac{\rho g H}{\rho_o}\frac{\partial \eta}{\partial y'} - \frac{H}{\rho_o}\frac{\partial P_a}{\partial y'} \\ &+ \frac{gH}{\rho_o}\frac{\partial H}{\partial y'}\int_\sigma^0 \sigma \frac{\partial \rho}{\partial \sigma} d\sigma - \frac{gH^2}{\rho_o}\frac{\partial}{\partial y'}\left[\int_\sigma^0 \rho d\sigma\right] + \frac{\partial \tau_{x'y'}}{\partial x'} + \frac{\partial}{\partial \sigma}\left[\frac{\partial \sigma}{\partial x}\tau_{x'y'}\right] \\ &+ \frac{\partial \tau_{y'y'}}{\partial y'} + \frac{\partial}{\partial \sigma}\left[\frac{\partial \sigma}{\partial y}\tau_{y'y'}\right] + H^{-1}\frac{\partial}{\partial \sigma}\left[K_m \frac{\partial v}{\partial \sigma}\right]\end{aligned}$$

Table 2.1. (continued) Internal-Mode Sigma Stretched Hydrodynamic Equations

(I.4) Temperature

$$\frac{\partial(HT)}{\partial t} + \frac{\partial(HuT)}{\partial x'} + \frac{\partial(HvT)}{\partial y'} + \frac{\partial(\omega T)}{\partial \sigma} = \frac{\partial Q_{x'T}}{\partial x'}$$
$$+ \frac{\partial}{\partial \sigma}\left[\frac{\partial \sigma}{\partial x} Q_{x'T}\right] + \frac{\partial Q_{y'T}}{\partial y'} + \frac{\partial}{\partial \sigma}\left[\frac{\partial \sigma}{\partial y} Q_{y'T}\right] + H^{-1}\frac{\partial}{\partial \sigma}\left[K_H \frac{\partial T}{\partial \sigma}\right]$$

(I.5) Salinity

$$\frac{\partial(HS)}{\partial t} + \frac{\partial(HuS)}{\partial x'} + \frac{\partial(HvS)}{\partial y'} + \frac{\partial(\omega S)}{\partial \sigma} = \frac{\partial Q_{x'S}}{\partial x'}$$
$$+ \frac{\partial}{\partial \sigma}\left[\frac{\partial \sigma}{\partial x} Q_{x'S}\right] + \frac{\partial Q_{y'S}}{\partial y'} + \frac{\partial}{\partial \sigma}\left[\frac{\partial \sigma}{\partial y} Q_{y'S}\right] + H^{-1}\frac{\partial}{\partial \sigma}\left[K_H \frac{\partial S}{\partial \sigma}\right]$$

(I.6) Turbulent Kinetic Energy

$$\frac{\partial(q^2H)}{\partial t} + \frac{\partial(q^2Hu)}{\partial x'} + \frac{\partial(q^2Hv)}{\partial y'} + \frac{\partial(q^2\omega)}{\partial \sigma} = \frac{\partial Q_{x'q^2}}{\partial x'}$$
$$+ \frac{\partial}{\partial \sigma}\left[\frac{\partial \sigma}{\partial x} Q_{x'q^2}\right] + \frac{\partial Q_{y'q^2}}{\partial y'} + \frac{\partial}{\partial \sigma}\left[\frac{\partial \sigma}{\partial y} Q_{y'q^2}\right] + H^{-1}\frac{\partial}{\partial \sigma}\left[K_q \frac{\partial q^2}{\partial \sigma}\right]$$
$$+ 2\frac{K_m}{H}\left[\left(\frac{\partial u}{\partial \sigma}\right)^2 + \left(\frac{\partial v}{\partial \sigma}\right)^2\right] + \frac{2g}{\rho_o} K_H \frac{\partial \rho}{\partial \sigma} - \frac{2Hq^3}{B_1 \ell}$$

(I.7) Turbulent Macroscale

$$\frac{\partial(q^2\ell)}{\partial t} + \frac{\partial(q^2\ell Hu)}{\partial x'} + \frac{\partial(q^2\ell Hv)}{\partial y'} + \frac{\partial(q^2\ell\omega)}{\partial \sigma} = \frac{\partial Q_{x'q^2\ell}}{\partial x'}$$
$$+ \frac{\partial}{\partial \sigma}\left[\frac{\partial \sigma}{\partial x} Q_{x'q^2\ell}\right] + \frac{\partial Q_{y'q^2\ell}}{\partial y'} + \frac{\partial}{\partial \sigma}\left[\frac{\partial \sigma}{\partial y} Q_{y'q^2\ell}\right] + H^{-1}\frac{\partial}{\partial \sigma}\left[K_q \frac{\partial q^2\ell}{\partial \sigma}\right]$$
$$+ \frac{\ell E_1 g}{\rho_o} K_H \frac{\partial \rho}{\partial \sigma} - \frac{Hq^3}{B_1}\varpi + \ell E_1 \frac{K_m}{H}\left[\left(\frac{\partial u}{\partial \sigma}\right)^2 + \left(\frac{\partial v}{\partial \sigma}\right)^2\right]$$

Table 2.2. Internal-Mode Sigma Stretched Hydrodynamic Equations Supplemental Relations

(S.1) Sigma horizontal gradients

$$-H\frac{\partial\sigma}{\partial x} = \sigma\frac{\partial H}{\partial x'} + \frac{\partial\eta}{\partial x'}; \quad -H\frac{\partial\sigma}{\partial y} = \sigma\frac{\partial H}{\partial y'} + \frac{\partial\eta}{\partial y'};$$

(S.2) Stress components

$$\tau_{x'y'} = \tau_{y'x'} = A_M\left[\frac{\partial(uH)}{\partial y'} + \frac{\partial}{\partial\sigma}\left[Hu\frac{\partial\sigma}{\partial y}\right] + \frac{\partial(vH)}{\partial x'} + \frac{\partial}{\partial\sigma}\left[Hv\frac{\partial\sigma}{\partial x}\right]\right]$$

$$\tau_{x'x'} = 2A_M\left[\frac{\partial(uH)}{\partial x'} + \frac{\partial}{\partial\sigma}\left[Hu\frac{\partial\sigma}{\partial x}\right]\right]; \quad \tau_{y'y'} = 2A_M\left[\frac{\partial(vH)}{\partial y'} + \frac{\partial}{\partial\sigma}\left[Hv\frac{\partial\sigma}{\partial y}\right]\right]$$

(S.3) Velocity components

$$\frac{dx'}{dt} = u; \quad \frac{dy'}{dt} = v; \quad \omega = H\frac{d\sigma}{dt}$$

(S.4) Temperature and Salinity diffusive fluxes

$$Q_{x'T} = A_H\left[\frac{\partial(TH)}{\partial x'} + \frac{\partial}{\partial\sigma}\left[HT\frac{\partial\sigma}{\partial x}\right]\right]$$

$$Q_{y'T} = A_H\left[\frac{\partial(TH)}{\partial y'} + \frac{\partial}{\partial\sigma}\left[HT\frac{\partial\sigma}{\partial y}\right]\right]$$

$$Q_{x'S} = A_H\left[\frac{\partial(SH)}{\partial x'} + \frac{\partial}{\partial\sigma}\left[HS\frac{\partial\sigma}{\partial x}\right]\right]$$

$$Q_{y'S} = A_H\left[\frac{\partial(SH)}{\partial y'} + \frac{\partial}{\partial\sigma}\left[HS\frac{\partial\sigma}{\partial y}\right]\right]$$

Table 2.2. (continued) Internal-Mode Sigma Stretched Hydrodynamic Equations Supplemental Relations

(S.5) Turbulence fluxes

$$Q_{x'q^2} = A_H\left[\frac{\partial(q^2H)}{\partial x'} + \frac{\partial}{\partial\sigma}\left[Hq^2\frac{\partial\sigma}{\partial x}\right]\right]$$

$$Q_{y'q^2} = A_H\left[\frac{\partial(q^2H)}{\partial y'} + \frac{\partial}{\partial\sigma}\left[Hq^2\frac{\partial\sigma}{\partial y}\right]\right]$$

$$Q_{x'q^2\ell} = A_H\left[\frac{\partial(q^2\ell H)}{\partial x'} + \frac{\partial}{\partial\sigma}\left[Hq^2\ell\frac{\partial\sigma}{\partial x}\right]\right]$$

$$Q_{y'q^2\ell} = A_H\left[\frac{\partial(q^2\ell H)}{\partial y'} + \frac{\partial}{\partial\sigma}\left[Hq^2\ell\frac{\partial\sigma}{\partial y}\right]\right]$$

In order to obtain the external-mode equations, integrate the previously developed internal mode continuity and horizontal momentum equations over the sigma space, $\sigma \in [-1, 0]$. Prior to performing this integration, it is instructive to consider the following representations.

$$u = \bar{u} + u'; \quad v = \bar{v} + v' \tag{2.40}$$

where $(\bar{u}, \bar{v}) = \left[\int_{-1}^{0} u d\sigma, \int_{-1}^{0} v d\sigma\right]$ and $(\bar{u}', \bar{v}') = (0,0)$.

Also define $(\overline{u'u'}, \overline{v'v'}, \overline{u'v'}) = \left[\int_{-1}^{0} u'u' d\sigma, \int_{-1}^{0} v'v' d\sigma, \int_{-1}^{0} u'v' d\sigma\right]$.

Further observe that the integral over sigma space of a constant is equal to the constant. Since the limits of integration are fixed, the integral of a derivative is equal to the derivative of the integral. By integrating each term of the continuity equation and the two horizontal momemtum equations and noting $\omega(o) = \omega(-1) = 0$, obtain the external-mode equation set given in Table 2.3.

Table 2.3. External-Mode Equation Set

(E.1) Continuity

$$\frac{\partial \eta}{\partial t} + \frac{\partial (\overline{u}H)}{\partial x'} + \frac{\partial (\overline{v}H)}{\partial y'} = 0$$

(E.2) x'-Momentum

$$\frac{\partial (H\overline{u})}{\partial t} + \frac{\partial (H\overline{u}\overline{u})}{\partial x'} + \frac{\partial (H\overline{u'u'})}{\partial x'} + \frac{\partial (H\overline{u}\overline{v})}{\partial y'} + \frac{\partial (H\overline{u'v'})}{\partial y'} = fH\overline{v}$$
$$- \frac{\overline{\rho}}{\rho_o} gH \frac{\partial \eta}{\partial x'} - \frac{H}{\rho_o}\frac{\partial P_a}{\partial x'} + \frac{gH}{\rho_o}\frac{\partial H}{\partial x'}\int_{-1}^{0}\int_{\sigma'}^{0} \sigma \frac{\partial \rho}{\partial \sigma} d\sigma\, d\sigma' - \frac{gH^2}{\rho_o}\frac{\partial}{\partial x'}\left[\int_{-1}^{0}\int_{\sigma'}^{0} \rho\, d\sigma\, d\sigma'\right]$$
$$+ \frac{\tau_{xS}}{\rho_o} - \frac{\tau_{xb}}{\rho_o} + \frac{\partial}{\partial x'}\left[2\overline{A}_M \frac{\partial (\overline{u}H)}{\partial x'}\right] + \frac{\partial}{\partial y'}\left[\overline{A}_M\left[\frac{\partial (\overline{u}H)}{\partial y'} + \frac{\partial (\overline{v}H)}{\partial y'}\right]\right]$$

(E.3) y'-Momentum

$$\frac{\partial (H\overline{v})}{\partial t} + \frac{\partial (H\overline{v}\overline{u})}{\partial x'} + \frac{\partial (H\overline{v'u'})}{\partial x'} + \frac{\partial (H\overline{v}\overline{v})}{\partial y'} + \frac{\partial (H\overline{v'v'})}{\partial y'} = -fH\overline{u}$$
$$- \frac{\overline{\rho}}{\rho_o} gH \frac{\partial \eta}{\partial y'} - \frac{H}{\rho_o}\frac{\partial P_a}{\partial y'} + \frac{gH}{\rho_o}\frac{\partial H}{\partial y'}\int_{-1}^{0}\int_{\sigma'}^{0} \sigma \frac{\partial \rho}{\partial \sigma} d\sigma\, d\sigma' - \frac{gH^2}{\rho_o}\frac{\partial}{\partial y'}\left[\int_{-1}^{0}\int_{\sigma'}^{0} \rho\, d\sigma\, d\sigma'\right]$$
$$+ \frac{\tau_{yS}}{\rho_o} - \frac{\tau_{yb}}{\rho_o} + \frac{\partial}{\partial y'}\left[2\overline{A}_M \frac{\partial (\overline{v}H)}{\partial y'}\right] + \frac{\partial}{\partial x'}\left[\overline{A}_M\left[\frac{\partial (\overline{u}H)}{\partial y'} + \frac{\partial (\overline{v}H)}{\partial x'}\right]\right]$$

2.2. Finite Difference Approximation of Sigma Coordinate Equations

First, the finite difference operations for each computational mode are introduced. For the internal- mode time integration, a time step ΔT, is used, which corresponds to $M\Delta t$, where Δt represents the external-mode time integration time step and M is defined as the mode splitting factor. For the external-mode, consider the water surface elevation, $\eta_{i,j,m}$, the total water depth, $H_{i,j,m}$, the x velocity component, $\overline{u}_{i,j,m}$, and the y velocity component, $\overline{v}_{i,j,m}$, to comprise the computational variables at time step m. For the internal-mode, consider the (x',y',σ) velocity

components, $(u_{i,j,k,n}, v_{i,j,k,n}, \omega_{i,j,k,n})$, the turbulent kinetic energy, $q^2{}_{i,j,k,n}$, the turbulent macroscale, $(q^2\ell)_{i,j,k,n}$, salinity, $S_{i,j,k,n}$, temperature, $T_{i,j,k,n}$, and density, $\rho_{i,j,k,n}$, to comprise the computational variables at time step n. Note $n\Delta T = Mm\Delta t$. The computational domain in the horizontal plane is defined setting $1 \le i \le IM$ and $1 \le j \le JM$. In the vertical discretization, $k \in (1/2,\ KB\ -1/2)$ where $k = 1/2$ corresponds to the surface $(\sigma_{1/2} = 0)$ and $k = KB\text{-}1/2$ corresponds to the bottom $(\sigma_{KB-1/2} = -1)$.

The value of σ at the mid-level of each layer is approximated in the following manner.

$$\Delta\sigma_k = \sigma_{k-1/2} - \sigma_{k+1/2} > 0,\ k = 1,\ KBM1, \quad KBM1 = KB - 1, \tag{2.41a}$$

$$\sigma L_k = (\sigma_{k+1/2} + \sigma_{k-1/2}) / 2,\ k = 1,\ KBM1, \tag{2.41b}$$

where
$\Delta\sigma_k$ $\equiv$ kth layer thickness, and
σL_k $\equiv$ σ value of the mid-level of the kth layer.

The Arakawa (1966) C space staggered grid is used in each horizontal plane as shown in Figure 2.1. The averaging and difference operators are defined in Table 2.4 for the internal-mode and in Table 2.5 for the external-mode. Note that $O(g)^n$ denotes the operator is applied to quantity g at time level n. Initially, the vertical velocity determination is considered followed by the finite differencing of the internal-mode equations. Next, the finite difference formulation of the external-mode equations is presented.

Vertical Velocity Determination

Consider the numerical computation of the vertical velocity, ω, in the following manner. First set

$$\omega^n_{i,j,1/2} = 0.$$

Consider the following finite difference form of Equation (2.23).

$$\omega^n_{i,j,k-1/2} = \sum_{kk=1}^{k} (\delta_x(Hu)^n_{kk} + \delta_y(Hv)^n_{kk})\,\Delta\sigma_{kk} - \sigma_{k-1/2}\,\delta_T(a_T(\eta))^n \quad .$$

Since

$$\omega^n_{i,j,k-3/2} = \sum_{kk=1}^{k-1} (\delta_x(Hu)^n_{kk} + \delta_y(Hv)^n_{kk})\,\Delta\sigma_{kk} - \sigma_{k-3/2}\,\delta_T(a_T(\eta))^n \quad ,$$

subtract the second from the first to obtain

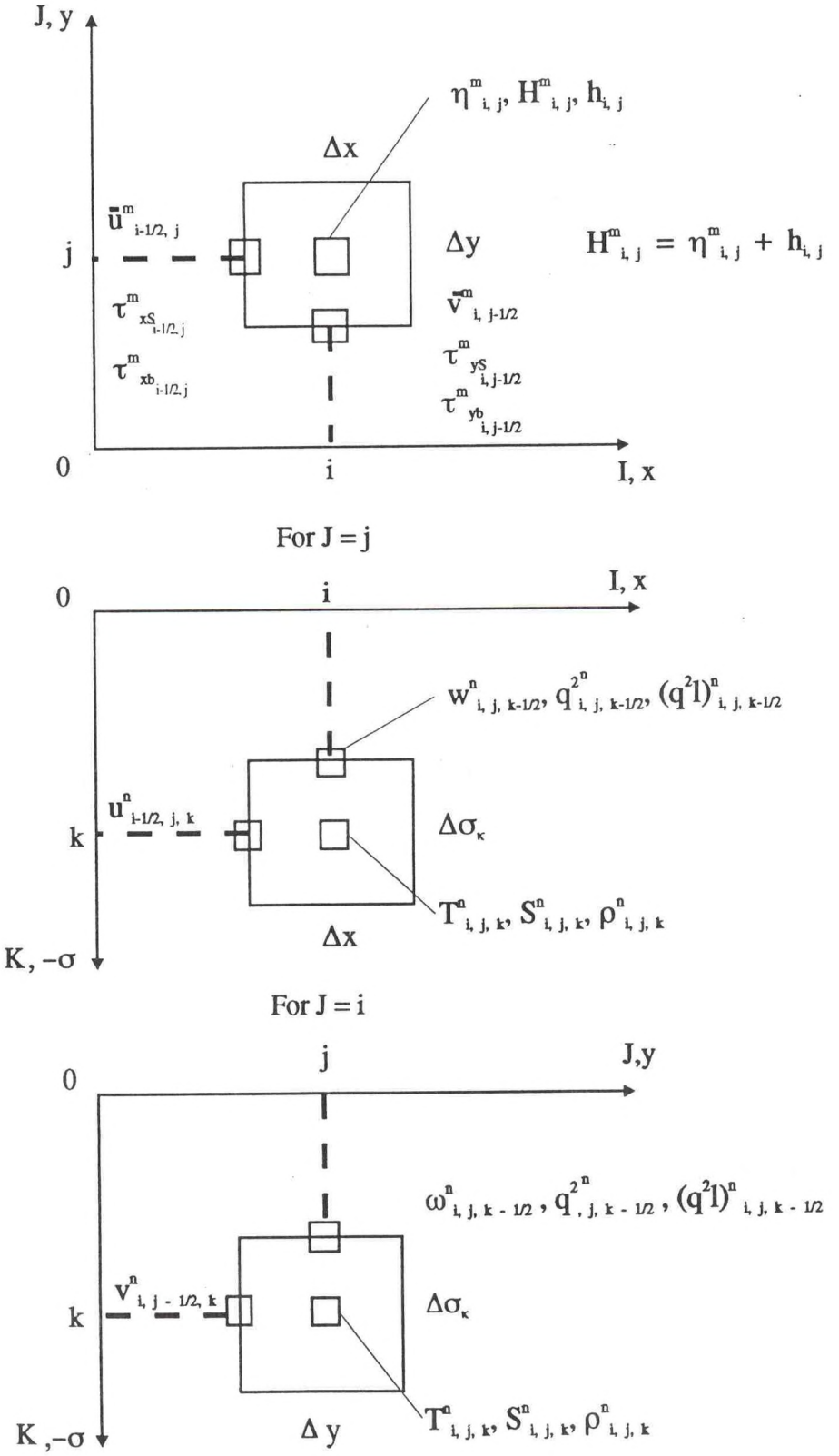

Figure 2.1. Staggered Grid System Indexing Structure

Table 2.4. Definition of Internal-Mode Averaging and Difference Operators

$$
\begin{aligned}
a_x(F_{i,j,k,n}) &= \frac{1}{2}\left(F_{i+1/2,j,k,n} + F_{i-1/2,j,k,n}\right) \\
a_y(F_{i,j,k,n}) &= \frac{1}{2}\left(F_{i,j+1/2,k,n} + F_{i,j-1/2,k,n}\right) \\
a_\sigma(F_{i,j,k,n}) &= \frac{1}{2}\left(F_{i,j,k+1/2,n} + F_{i,j,k-1/2,n}\right) \\
a_T(F_{i,j,k,n}) &= \frac{1}{2}\left(F_{i,j,k,n+1/2} + F_{i,j,k,n-1/2}\right) \\
\delta_x(F_{i,j,k,n}) &= \frac{F_{i+1/2,j,k,n} - F_{i-1/2,j,k,n}}{\Delta x} \\
\delta_y(F_{i,j,k,n}) &= \frac{F_{i,j+1/2,k,n} - F_{i,j-1/2,k,n}}{\Delta y} \\
\delta_\sigma(F_{i,j,k,n}) &= \frac{F_{i,j,k-1/2,n} - F_{i,j,k+1/2,n}}{\Delta \sigma} \\
\delta_T(F_{i,j,k,n}) &= \frac{F_{i,j,k,n+1/2} - F_{i,j,k,n-1/2}}{\Delta T} \\
\delta_x(a_x(F_{i,j,k,n})) &= \frac{\frac{1}{2}\left[\left(F_{i+1,j,k,n} + F_{i,j,k,n}\right) - \left(F_{i,j,k,n} + F_{i-1,j,k,n}\right)\right]}{\Delta x} \\
\delta_y(a_y(F_{i,j,k,n})) &= \frac{\frac{1}{2}\left[\left(F_{i,j+1,k,n} + F_{i,j,k,n}\right) - \left(F_{i,j,k,n} + F_{i,j-1,k,n}\right)\right]}{\Delta y} \\
\delta_\sigma(a_\sigma(F_{i,j,k,n})) &= \frac{\frac{1}{2}\left[\left(F_{i,j,k-1,n} + F_{i,j,k,n}\right) - \left(F_{i,j,k,n} + F_{i,j,k+1,n}\right)\right]}{\Delta \sigma} \\
a_{xy}(F_{i,j,k,n}) &= a_x(a_y(F_{i,j,k,n})) = a_y(a_x(F_{i,j,k,n})) \\
a_{x\sigma}(F_{i,j,k,n}) &= a_x(a_\sigma(F_{i,j,k,n})) = a_\sigma(a_x(F_{i,j,k,n})) \\
a_{y\sigma}(F_{i,j,k,n}) &= a_y(a_\sigma(F_{i,j,k,n})) = a_\sigma(a_y(F_{i,j,k,n}))
\end{aligned}
$$

$$
\omega^n_{i,j,k-1/2} = \omega^n_{i,j,k-3/2} + \left(\delta_x(Hu)^n_k + \delta_y(Hv)^n_k\right)\Delta\sigma_k + \Delta\sigma_{k-1}\,\delta_T(a_T(\eta))^n \tag{2.42}
$$

where $k \in (2, KB)$. Note $\omega^n_{i,j,KB-1/2}$ should equal zero and differs only due to truncation error.

Table 2.5. Definition of External-Mode Averaging and Difference Operators

$$a_x(F_{i,j,m}) = \frac{1}{2}(F_{i+1/2,j,m} + F_{i-1/2,j,m})$$

$$a_y(F_{i,j,m}) = \frac{1}{2}(F_{i,j+1/2,m} + F_{i,j-1/2,m})$$

$$a_t(F_{i,j,m}) = \frac{1}{2}(F_{i,j,m+1/2} + F_{i,j,m-1/2})$$

$$\delta_x(F_{i,j,m}) = \frac{F_{i+1/2,j,m} - F_{i-1/2,j,m}}{\Delta x}$$

$$\delta_y(F_{i,j,m}) = \frac{F_{i,j+1/2,m} - F_{i,j-1/2,m}}{\Delta y}$$

$$\delta_t(F_{i,j,m}) = \frac{F_{i,j,m+1/2} - F_{i,j,m-1/2}}{\Delta t}$$

$$\delta_x(a_x(F_{i,j,m})) = \frac{\frac{1}{2}\left[(F_{i+1,j,m} + F_{i,j,m}) - (F_{i,j,m} + F_{i-1,j,m})\right]}{\Delta x}$$

$$\delta_y(a_y(F_{i,j,m})) = \frac{\frac{1}{2}\left[(F_{i,j+1,m} + F_{i,j,m}) - (F_{i,j,m} + F_{i,j-1,m})\right]}{\Delta y}$$

$$a_{xy}(F_{i,j,m}) = a_x(a_y(F_{i,j,m})) = a_y(a_x(F_{i,j,m}))$$

Internal-Mode Equations

The finite difference form of the continuity equation (I.1) at *(i,j,k,n)* is

$$\delta_T(a_T(\eta)) + \delta_x(a_x(H)u) + \delta_y(a_y(H)v) + \delta_\sigma(\omega) = 0 \quad . \tag{2.43}$$

In the following two motion equations, the horizontal viscosity terms are designated as F_x^{n-1} and F_y^{n-1} after Blumberg and Mellor (1987). Similarly, in the three constituent equations for θ = (S,T), q^2, and $q^2\ell$, the horizontal diffusion terms are designated using Blumberg and Mellor's (1987) notation as F_θ^{n-1}, F_q^{n-1}, and F_ℓ^{n-1}, respectively. Next, the finite difference forms are explicitly stated for these terms, which are not provided in their article.

The u-motion equation (I.2) at *(i-1/2, j, k,n)* is

$$\begin{aligned}
&\delta_T(a_T(\, a_x(H)\, u\,)\,) + \delta_x\,(a_x(\, a_x(H)u\,)a_x(u)\,) + \delta_y\,(a_x(\, a_y(H)v)a_y(u)\,) \\
&- a_x(\, fa_y(v)H) + \delta_\sigma(\, a_x(\omega)\; a_\sigma(u)\,) + g\, a_x(H)\delta_x(\eta) \qquad (2.44)\\
&= \delta_\sigma\,(\frac{a_x(K_M)}{a_x(H)}\;\delta_\sigma(u)\,)^{n+1} - \frac{g(\, a_x(H)\,)^2}{\rho_o}\,\delta_x(\sum_{r=1}^{k}\; a_\sigma(\rho_{r-\frac{1}{2}}\;\; a_\sigma(\Delta\;\sigma_{r-\frac{1}{2}}))\\
&+ \frac{g\, a_x(H)}{\rho_o}\,\delta_x(H)\;(\sum_{r=1}^{k}\;\sigma_r\; a_x(\,\delta_\sigma(\rho_{r-\frac{1}{2}}\,)\,)\;\Delta\,\sigma_{r-\frac{1}{2}}\,) + F_x^{n-1}
\end{aligned}$$

where,

$$F_x^{n-1} \;=\; \delta_x\left(2\,A_M\,H\,\delta_x(u)\right)^{n-1} + \delta_y\left(a_{xy}(A_M)\,a_{xy}(H)\left(\delta_y(u) + \delta_x(v)\right)\right)^{n-1} .$$

The v-motion equation (I.3) at *(i,j-1/2,k,n)* is

$$\begin{aligned}
&\delta_T(\, a_T(\, a_y(H)\; v\,)) + \delta_x(\, a_y(a_x(H)\; u)\; a_x(v)\,) + \delta_y(\, a_y(a_y(H)\; v)\; a_y(v)\,) \\
&+ a_y(\, f\, a_x(u)\; H) + \delta_\sigma(\, a_y(\omega)\; a_\sigma(v)\,) + g\, a_y(H)\;\delta_y(\eta) \qquad (2.45)\\
&= \delta_\sigma\,(\frac{a_y(K_M)}{a_y(H)}\;\delta_\sigma(\; v)\,)^{n+1} - \frac{g(\, a_y(H)\,)^2}{\rho_o}\,\delta_y(\sum_{r=1}^{k}\; a_\sigma(\rho_{r-\frac{1}{2}})\;\; a_\sigma(\Delta\;\sigma_{r-\frac{1}{2}})\,)\\
&+ \frac{g\, a_y(H)}{\rho_o}\,\delta_y(H)\;(\sum_{r=1}^{k}\;\sigma_r\; a_y(\delta_\sigma(\,\rho_{r-\frac{1}{2}}\,))\,\sigma_{r-\frac{1}{2}}\,) + \;F_y^{n-1}
\end{aligned}$$

where,

$$F_y^{n-1} \;=\; \delta_y\left(2\,A_M\,H\,\delta_y(v)\right)^{n-1} + \delta_x\left(a_{yx}(A_M)\,a_{yx}(H)\left(\delta_y(u) + \delta_x(v)\right)\right)^{n-1} .$$

The salinity (*S*) and temperature (*T*) equations at *(i,j,k,n)* where $\theta \equiv S$ or T are

$$\begin{aligned}
&\delta_T\left(a_T(\theta\, H)\right) + \delta_x\left(a_x(\theta)\; u\; a_x(H)\;\right) + \delta_y\left(\; a_y(\theta)\; v\; a_y(H)\;\right) + \delta_\sigma\left(\; a_\sigma(\theta)\;\omega\right)\\
&= \;\delta_\sigma(\frac{K_H}{H}\;\delta_\sigma\theta\,)^{n+1} + F_\theta^{n-1} \qquad (2.46)
\end{aligned}$$

where,

$$F_\theta^{n-1} \;=\; \delta_x\left(a_x(A_H)\; a_x(H)\;\delta_x(\,\theta\,)\right)^{n-1} + \delta_y\left(a_y(A_H)\; a_y(H)\;\delta_y(\,\theta\,)\right)^{n-1} .$$

The turbulent kinetic energy equation at *(i,j,k-1/2,n)* is

$$\begin{aligned}
&\delta_T\left(a_T(q^2 H)\right) + \delta_x\left(a_\sigma(u)\ a_x(q^2)\ a_x(H)\ \right) + \delta_y\left(a_\sigma(v)\, a_y(q^2)\ a_y(H)\ \right) + \delta_\sigma\left(a_\sigma(\omega)\ a_\sigma(q^2)\ \right) \\
&= \delta_\sigma\left(\frac{a_\sigma(K_q)}{H}\ \delta_\sigma(q^2)\right)^{n+1} + \frac{2K_m}{H}\left[\left(\delta_\sigma a_x(u)\right)^2 + \left(\delta_\sigma a_y(v)\right)^2\right] \\
&+ \frac{2g}{\rho_0} K_H \delta_\sigma \rho - \frac{2Hq^3}{B_1 \ell} + F_q^{n-1}
\end{aligned} \tag{2.47}$$

where,

$$F_q^{n-1} = \delta_x\left(a_{x\sigma}(A_H)\, a_x(H)\ \delta_x(q^2)\right)^{n-1} + \delta_y\left(a_{y\sigma}(A_H)\, a_y(H)\ \delta_y(q^2)\right)^{n-1} .$$

The turbulent macroscale at *(i,j,k-1/2,n)* is

$$\begin{aligned}
&\delta_T\left(a_T(q^2 \ell H)\right) + \delta_x\left(a_\sigma(u)\ a_x(q^2\ell) a_x(H)\right) + \delta_y\left(a_\sigma(v)\, a_y(q^2\ell)\ a_y(H)\ \right) + \delta_\sigma\left(a_\sigma(\omega)\ a_\sigma(q^2\ell)\ \right) \\
&= \delta_\sigma\left(\frac{a_\sigma(K_q)}{H}\ \delta_\sigma q^2\ell\right)^{n+1} + \ell E_1 \frac{K_m}{H}\left[\left(\delta_\sigma a_x(u)\right)^2 + \left(\delta_\sigma a_y(v)\right)^2\right] \\
&+ \frac{\ell E_1 g}{\rho_0} K_H \delta_\sigma \rho - \frac{Hq^3}{B_1}\varpi + F_\ell^{n-1}
\end{aligned} \tag{2.48}$$

where,

$$F_\ell^{n-1} = \delta_x\left(a_{x\sigma}(A_H)\, a_x(H)\ \delta_x(q^2\ell)\right) + \delta_y\left(a_{y\sigma}(A_H)\, a_y(H)\ \delta_y(q^2\ell)\right) .$$

External-Mode Equations

The continuity equation at *(i,j,m)* is

$$\delta_t\left(a_t(\eta)\ \right) + \delta_x\left(a_x(H)\ \bar{u}\right) + \delta_y\left(a_y(H)\ \bar{v}\right) = 0 . \tag{2.49}$$

In the two vertically averaged momentum equations, the horizontal viscosity and vertical structure terms are designated after Blumberg and Mellor (1987) as $(\bar{F}_x, \bar{F}_y)$ and (Φ_x, Φ_y), respectively. The complete finite difference forms are not given in their article and are therefore provided here.

The $\bar{u}$ - momentum equation at *(i-1/2,j,m)* is

$$\delta_t\left(a_t(a_x(H)\ \bar{u})\ \right) + \delta_x\left(a_x(a_x(H)\ \bar{u})\ a_x(\bar{u})\ \right) + \delta_y\left(a_x(a_y(H)\ \bar{v})\ a_y(\bar{u})\ \right)$$
$$- a_x(f\ a_y(\bar{v})H) + g a_x(H)\ \delta_x(\eta) - \bar{F}_x^{m-1} = \Phi_x^n \qquad (2.50)$$

where,

$$\bar{F}_x^{m-1} = \delta_x\left(2\bar{A}_M\ H\ \delta_x(\bar{u})\right)^{m-1} + \delta_y\left(a_{xy}(\bar{A}_M)\ a_{xy}(H)\left(\delta_x(\bar{v}) + \delta_y(\bar{u})\right)\right)^{m-1}$$

and

$$\Phi_x^n = -\delta_x\left(a_x(a_x(H)\ u)\ a_x(u)\ \right)^n - \delta_y\left(a_x(a_y(H)\ v)\ a_y(u)\ \right)^n$$
$$+ \delta_x\left(a_x(a_x(H)\ \bar{u})\ a_x(\bar{u})\ \right)^n + \delta_y\left(a_x(a_y(H)\ \bar{v})\ a_y(\bar{u})\ \right)^n$$
$$+ \delta_x\left(2\,A_M\,H\,\delta_x(u)\right)^n + \delta_y\left(a_{xy}(A_M)\ a_{xy}(H)\left(\delta_y(u) + \delta_x(v)\right)\right)^n$$
$$- \delta_x\left(2\,\bar{A}_M\,H\,\delta_x(\bar{u})\right)^n - \delta_y\left(a_{xy}(\bar{A}_M)\ a_{xy}(H)\left(\delta_y(\bar{u}) + \delta_x(\bar{v})\right)\right)^n$$
$$- g\,\frac{\left(a_x(H)^n\right)^2}{\rho_o}\sum_{k=1}^{KB-1}\delta_x\left[\sum_{r=1}^{k} a_o(\rho_{r-1/2})\ a_o(\Delta\sigma_{r-1/2})\ \right]^n$$
$$+ \frac{g\ a_x(H)^n}{\rho_o}\,\delta_x(H)\sum_{k=1}^{KB-1}\left[\sum_{r=1}^{k}\sigma_r\ a_x(\delta_\sigma\left(\rho_{r-1/2}\right))^n\Delta\sigma_{r-1/2}\right]^n \quad .$$

The $\bar{v}$ - momentum equation at *(i,j-1/2,m)* is (2.51)

$$\delta_t\left(a_t(a_y(H)\ \bar{v})\ \right) + \delta_x\left(a_y(a_x(H)\ \bar{u})\ a_x(\bar{v})\right)\ \right) + \delta_y\left(a_y(a_y(H)\ \bar{v})\ a_y(\bar{v})\ \right)$$
$$+ a_y(f\ a_x(\bar{u})H) + g a_y(H)\ \delta_y(\eta) - \bar{F}_y^{m-1} = \Phi_y^n$$

where,

$$\bar{F}_y^{m-1} = \delta_y\left(2\bar{A}_M\ H\ \delta_y(\bar{v})\right)^{m-1} + \delta_x\left(a_{yx}(\bar{A}_M)\ a_{yx}(H)\ \left(\delta_x(\bar{v}) + \delta_y(\bar{u})\right)\right)^{m-1}$$

and

$$\Phi_y^n = -\delta_x\left(a_y(a_x(H)\ u)\ a_x(v)\ \right)^n - \delta_y\left(a_y(a_y(H)\ v)\ a_y(v)\ \right)^n$$
$$+ \delta_x\left(a_y(a_x(H)\ \bar{u})\ a_x(\bar{v})\ \right)^n + \delta_y\left(a_y(a_y(H)\ \bar{v})\ a_y(\bar{v})\ \right)^n$$
$$+ \delta_x\left(a_{yx}(A_M)\ a_{yx}(H)\ \left(\delta_y(u) + \delta_x(v)\right)\right)^n + \delta_y\left(2A_M\,H\,\delta_y(v)\right)^n$$
$$- \delta x\left(a_{yx}(\bar{A}_M)\ \ a_{yx}(H)\ \ \left(\delta_x(\bar{v}) + \delta_y(\bar{u})\right)\right)^n - \delta_y\left(2\,\bar{A}_M\,H\,\delta_y(\bar{v})\right)^n$$
$$- g\,\frac{\left(a_y(H)^n\right)^2}{\rho_o}\sum_{k=1}^{KB-1}\delta_y\left[\sum_{r=1}^{k} a_o(\rho_{r-1/2})\ a_o(\Delta\sigma_{r-1/2})\ \right]^n$$
$$+ \frac{g\ a_y(H)^n}{\rho_o}\,\delta_y(H)\sum_{k=1}^{KB-1}\left[\sum_{r=1}^{k}\sigma_r\ a_y(\delta_\sigma\left(\rho_{r-1/2}\right))\Delta\sigma_{r-1/2}\right]^n \quad .$$

2.3. Numerical Solution Techniques

The computational strategy is to solve the external-mode equations in Table 2.3 using an explicit finite difference scheme with a short time step (Δt) to resolve tidal motions. The external mode solutions are obtained with the vertically dependent horizontal viscosity and pressure terms (Φ_x^n, Φ_y^n) held fixed in time. Then the internal-mode equations of Table 2.1 are solved using an explicit finite difference scheme for the continuity equation. The vertical eddy viscosity as well as the bottom friction terms in the two horizontal momentum equations are treated implicitly, while all other terms are handled explicitly in the finite difference representations. Similarly, the vertical diffusion terms in the salinity, temperature, turbulent kinetic energy, and turbulent macroscale equations are treated implicitly, while all other terms are explicitly evaluated in the finite difference approximations. The internal-mode equations are solved on a large time step (ΔT) with the external mode providing the $\partial\eta/\partial x'$ and $\partial\eta/\partial y'$ terms in the momemtum equations. Once the vertical structure has been solved, the vertically dependent terms in the external-mode equations are updated and the external mode is solved. The process repeats over the duration of the simulation, which is specified in terms of a certain number of internal-mode time steps. The leap frog time differencing introduces a tendency for the solution at even and odd time steps to split. In order to reduce the time splitting, a weak filter (Asselin, 1972) is used to smooth the solution.

The following stability conditions are used to limit the external- and internal-mode time steps.

External-mode

$$\Delta t_E^1 = \frac{1}{C_t^E}\left[\frac{1}{\Delta x^2} + \frac{1}{\Delta y^2}\right]^{-0.5} = \frac{1}{C_t^E}\left[\frac{\Delta y^2 + \Delta x^2}{\Delta x^2\,\Delta y^2}\right]^{-0.5} = \frac{1}{C_t^E}\frac{\Delta x\,\Delta y}{\sqrt{\Delta x^2 + \Delta y^2}} \qquad (2.52)$$

with $C_t^E = 2\sqrt{gH} + \bar{u}_{max}$, where $\bar{u}_{max}$ is the maximum vertically averaged velocity expected.

A rotational condition must also be satisfied of the form

$$\Delta t_E^2 = f^{-1} = (2\Omega \sin\theta)^{-1}, \qquad (2.53)$$

where Ω is the angular velocity of the earth, and θ is the latitude of the center of the computational grid.

Next set $\Delta t_E = \min(\Delta t_E^1, \Delta t_E^2)$. Then, $\Delta t < \Delta t_E$.

Internal-mode

$$\Delta T_I^1 = \frac{1}{C_t^I}\left[\frac{1}{\Delta x^2} + \frac{1}{\Delta y^2}\right]^{-0.5} \text{ with } C_t^I = 2C + U_{max} \ , \qquad (2.54)$$

$$C = \sqrt{g H \frac{\Delta \rho}{\rho_o}} \quad , \quad \text{and} \quad U_{\max} = \left(u_{\max}^2 + v_{\max}^2 \right)^{1/2} \quad .$$

If grid cell Reynolds numbers, $\frac{(\Delta x)\, u_{\max}}{A_H}$, $\frac{(\Delta y)\, v_{\max}}{A_H}$ are on the order of 1, the following time constraint must be obeyed.

$$\Delta T_I^2 = \frac{1}{4 A_H} \left(\frac{1}{\Delta x^2} + \frac{1}{\Delta y^2} \right)^{-1} \quad . \tag{2.55}$$

Consider $\Delta T_I = \min(\Delta T_I^1 , \Delta T_I^2)$. Then , $\Delta T < \Delta T_I$.

3. MODEL ENHANCEMENTS

To enable long term computation of residual circulation for input to the water quality component of the study, it was necessary to develop both a restart capability and a suitable time averaging scheme for determining mass conserving residual circulation fields. The techniques employed for restarting are outlined in Section 3.1 and for residual circulation in Section 3.2. To include the influence of sewage treatment plant inflows, combined sewer overflows, and New York State streams on the salinity structure in western Long Island Sound, the point source methodology for flow input outlined in Section 3.3 was developed. The techniques employed for computing tidal statistics are developed in Section 3.4.

3.1. Restart Mechanics

To restart the simulation, the external-mode horizontal velocity components and water surface elevation at the current and previous time steps are saved at the end of the run. For the internal-mode, the current time step bottom stress components and vertical mixing coefficients, and the current and previous time step water surface elevation, horizontal velocity components, salinity, and temperature are saved. Both external- and internal-mode variables are read in to initialize the solution for restarting the next run.

The restarting procedure is not fully dynamic in the sense that the procedures introduce slight differences between field variables obtained from initial and restarted solutions at corresponding time points in the initial time period of the restart time. Differences rapidly decay for times outside this neighborhood and the procedures are considered sufficiently robust but are termed quasi-dynamic.

3.2. Residual Circulation

The Lagrangian residual circulation is defined as the sum of the Eulerian residual circulation and the Stokes drift by Longuet-Higgins (1969). Hamrick (1990) has represented the Stokes drift as the curl of a velocity vector potential in the following manner. In vector form (bold font),

$$\boldsymbol{u}_L = \boldsymbol{u}_E + \nabla \times \boldsymbol{B} \tag{3.1}$$

where

$\boldsymbol{u}_L$ $\equiv$ Lagrangian residual circulation,
$\boldsymbol{u}_E$ $\equiv$ Eulerian residual circulation,
$\nabla \times \boldsymbol{B}$ $\equiv$ Stokes drift (curl of velocity vector potential).

Note that $\nabla \cdot \boldsymbol{u}_L = \nabla \cdot \boldsymbol{u}_E$, since $\nabla \cdot (\nabla \times \boldsymbol{B}) = 0$.

Letting $\langle T \rangle$ correspond to a 24.84 hour (twice the M_2 tidal period) average of T, then the velocity vector potential, $\boldsymbol{B}$, is given by the following form.

$$B_1 = \langle v \int_0^t \omega \, dt \rangle_T - \langle vt \rangle_T \langle \omega \rangle_T \tag{3.2a}$$

$$B_2 = \langle \omega \int_0^t u \, dt \rangle_T - \langle \omega t \rangle_T \langle u \rangle_T \tag{3.2b}$$

$$B_3 = \langle u \int_0^t v \, dt \rangle_T - \langle ut \rangle_T \langle v \rangle_T \tag{3.2c}$$

with $\boldsymbol{B} = (B_1 , B_2 , B_3)$.

Consider the incremental volume, $\Delta x \Delta y H \Delta \sigma$, then mass fluxes may be written as follows

$$\boldsymbol{Q_L} = \boldsymbol{Q_E} + \nabla x \boldsymbol{B'}, \tag{3.3}$$

with

$$\boldsymbol{Q_E} = \left(\Delta\sigma\Delta y \langle Hu \rangle_T , \Delta\sigma\Delta x \langle Hv \rangle_T , \Delta x \Delta y \langle \omega \rangle_T \right) \text{ and} \tag{3.4a}$$

$$\boldsymbol{B'} = \left(\Delta\sigma\Delta y \langle H \rangle_T B_1 , \Delta\sigma\Delta x \langle H \rangle_T B_2 , \Delta x \Delta y B_3 \right) . \tag{3.4b}$$

Using Equation (3.4), the following hydrodynamic variables are computed and written to a transfer file.

$\langle Hu \rangle_T$	≡	time-averaged horizontal flux per unit width in x-direction,
$\langle Hv \rangle_T$	≡	time-averaged horizontal flux per unit width in y-direction,
$\langle \omega \rangle_T$	≡	time-averaged vertical flux,
$\boldsymbol{B'}$	≡	velocity vector potential,
$\langle S \rangle_T$	≡	time-averaged salinity,
$\langle T \rangle_T$	≡	time-averaged temperature,
$\langle A_H \rangle_T$	≡	time-averaged horizontal diffusivity,
$\langle K_H \rangle_T$	≡	time-averaged vertical diffusivity, and
$\langle H \rangle_T$	≡	time-averaged water depth.

In regions of sharp gradients in topography and in one-dimensional grid sections, particularly in the vicinity of corners, the vector potential computation is problematic and may require significant spatial smoothing. To eliminate this concern, a one-hour averaging period was used. Therefore, the Eulerian velocity field may be used directly to estimate the residual circulation.

3.3. Specification of a Point Source Freshwater Inflow

Freshwater inflow can be produced by rivers, sewage treatment plants, and combined sewer overflows. Sewage treatment plant inflows were considered time invariant. Seventeen time varying (monthly) combined sewer overflows were developed by EPA based upon rainfall-runoff models and six small New York stream discharges (average daily) were included in the model. To implement each of these inflows, it was necessary to modify the external-mode continuity equation, the internal-mode continuity equation, and the internal-mode salinity and temperature transport equations as outlined in turn below.

The External-Mode Continuity Equation

Consider *nstp* sewage treatment plant inflows with volumetric inflow rates, $Q_{i,j}^{STP}$, specified for $(i,j) \in \{(istp_n, jstp_n),\ n = 1,\ nstp\}$. Similarly, consider *ncso* combined sewer overflow volumetric rates, $Q_{i,j}^{CSO}$, specified at $(i,j) \in \{(icso_n, jcso_n),\ n = 1,\ ncso\}$ and *nyr* New York State streamflows, $Q_{i,j}^{NYR}$, specified at $(i,j) \in \{(inyr_n, jnyr_n),\ n = 1,\ nyr\}$. The continuity equation (2.32) is modifed in the following manner.

$$\delta_t \left(a_t(\eta) \right) + \delta_x \left(a_x(H)\, \bar{u} \right) + \delta_y \left(a_y(H)\, \bar{v} \right) = z_{i,j}^{STP} + z_{i,j}^{CSO} + z_{i,j}^{NYR} \tag{3.5}$$

where

$$z_{i,j}^{STP} = \left\{ \begin{array}{rl} 0 & i,j \notin \left\{ (istp_n, jstp_n),\ n = 1,\ nstp \right\} \\ Q_{i,j}^{STP}/(\Delta x \Delta y) & i,j \in \left\{ (istp_n, jstp_n),\ n = 1,\ nstp \right\} \end{array} \right\} .$$

Corresponding relationships hold for $z_{i,j}^{CSO}$ and $z_{i,j}^{NYR}$.

Internal-Mode Continuity Equation

The right-hand side of the continuity equation Equation (2.26) is modified as follows.

$$\begin{aligned} &\delta_T \left(a_T(\eta) \right) + \delta_x \left(a_x(H)\, u \right) + \delta_y \left(a_y(H)\, v \right) + \delta_\sigma \left(\omega \right) \\ &= z_{i,j,k}^{STP} + z_{i,j,k}^{CSO} + z_{i,j,k}^{NYR} \end{aligned} \tag{3.6}$$

with

$$z_{i,j,k}^{STP} = \left\{ \begin{array}{rl} 0 & i,j \notin \left\{ (istp_n, jstp_n), \ n = 1, \ nstp \right\} \\ Q_{i,j}^{STP} \ d_k^{STP}/(\Delta x \Delta y) & i,j \in \left\{ (istp_n, jstp_n), \ n = 1, \ nstp \right\} \end{array} \right\}$$

$$d_k^{NYR} = d_k^{CSO} = \left\{ \begin{array}{ll} 0 & k = 0 \\ 1 & k = 1 \end{array} \right\}$$

$$d_k^{STP} = \left\{ \begin{array}{ll} 0 & k < KBM1 \\ 1 & k = KBM1 \end{array} \right\} .$$

Corresponding relationships hold for $z_{i,j,k}^{CSO}$ and $z_{i,j,k}^{STP}$.

Thus the layer inflow locations are specified such that the sewage treatment plant flows are input to the bottom layer, while the combined sewer overflows and New York state streamflows are input to the surface layer.

Salinity and Temperature Transport Equations

The following transport equation (modified from Equation (2.29)) is used for $\theta \in$ (S,T).

$$\begin{aligned} & \delta_t \left(\overline{\theta H}^t \right) + \delta_x \left(\overline{\theta}^x \ u \ \overline{H}^x \right) + \delta_y \left(\overline{\theta}^y v \ \overline{H}^y \right) + \delta_\sigma \left(\overline{\sigma}^\sigma \omega \right) \\ & = \delta_\sigma \left[\frac{K_H}{H} \delta_\sigma \theta \right]^{n+1} + F_\theta^{n-1} + S_{i,j,k}^{STP} + S_{i,j,k}^{CSO} + S_{i,j,k}^{NYR} \end{aligned} \tag{3.7}$$

with

$$S_{i,j,k}^{STP} = \left\{ \begin{array}{rl} 0 & i,j \notin \left\{ (istp_n, jstp_n), \ n = 1, \ nstp \right\} \\ Q_{i,j,k}^{STP} \ CS_{i,j,k}^{STP}/(\Delta x \Delta y) & i,j \in \left\{ (istp_n, jstp_n), \ n = 1, \ nstp \right\} \end{array} \right\} .$$

$S_{i,j,k}^{CSO}$ and $S_{i,j,k}^{NYR}$ are defined similarly.

Salinity values are considered zero for all inflows, while inflow temperatures are set equal to the most recent grid cell values as indicated below.

$$CS_{i,j,k}^{STP} = CS_{i,j,k}^{CSO} = CS_{i,j,k}^{NYR} = 0. \text{ psu for } \theta \equiv S \ ,$$

$$CS_{i,j,k}^{STP} = CS_{i,j,k}^{CSO} = CS_{i,j,k}^{NYR} = T_{i,j,k}^{n-1} \ . \ ^oC \text{ for } \theta \equiv T \ ,$$

and

$$Q_{i,j,k}^{STP} = Q_{i,j}^{STP} \ d_k^{STP} \ ,$$

$$Q_{i,j,k}^{CSO} = Q_{i,j}^{CSO} \ d_k^{CSO} \ ,$$

$$Q_{i,j,k}^{NYR} = Q_{i,j}^{NYR} \ d_k^{NYR} \ .$$

3.4. Tidal Statistics

The following set of tidal statistics was developed to verify the tidal characteristics at regular intervals throughout long-term simulation. The phase is relative to an M_2 tidal period.

$EMAX_{i,j}$ ≡ maximum water surface elevation in cell (i,j),
$EMIN_{i,j}$ ≡ minimum water surface elevation in cell (i,j),
$EPHSMX_{i,j}$ ≡ phase (°) of maximum elevation in cell (i,j),
$EPHSMN_{i,j}$ ≡ phase (o) of minimum elevation in cell (i,j),
$VFLD_{i,j}$ ≡ maximum flood current (vertically averaged) in cell (i,j),
$VEBB_{i,j}$ ≡ maximum ebb current (vertically averaged) in cell (i,j),
$VPHSMX_{i,j}$ ≡ phase (°) of maximum flood current in cell (i,j), and
$VPHSMN_{i,j}$ ≡ phase (°) of maximum ebb current in cell (i,j).

These statistics also served as a basis on which to develop the necessary tidal atlas statistics as discussed in Volume 2.

An M_2 clock using local standard time as a reference was used as defined in the following relationship.

$$T(M_2) = C(t - t_d) \tag{3.8}$$

where

$T(M_2)$ ≡ number of M_2 tidal cycles elapsed from January 1 hour 00 1988 EST,
C ≡ number of M_2 tidal cycles per Julian day (1.93227361),
t ≡ time in Julian days relative to January 1 hour 00 1988 EST, and
t_d ≡ Julian day offset (0 in this case).

The user specifies a given number of M_2 tidal cycles after which the above statistics are computed over each subsequent M_2 tidal cycle.

4. MODEL APPLICATION TO LONG ISLAND SOUND

The Long Island Sound three-dimensional hydrodynamic model as documented in the previous sections has been employed to simulate tidal and residual circulation and salinity and temperature distribution in Long Island and Block Island Sounds. Tidal circulation has been studied by Sun (1992) and initial thermohaline simulations have been presented by Wei (1992) and Schmalz (1992). The development of a tidal elevation and current atlas is presented in Volume 2. Residual circulation and salinity and temperature distributions were simulated initially for the nine month calibration period, April - December 1988, which constituted the initial nine months of an eighteen month simulation. The remaining nine month period, January - September 1989, was considered as an independent verification period. Residual and thermohaline circulation are compared with observational data in Volume 3: Thermohaline and Residual Circulation. The grid development and associated stability issues, initial conditions, boundary conditions, and overall computational requirements are presented below.

4.1. Grid Development

A 2 km (2032 m) uniform horizontal cell size was employed to form the computational grid extending from The Battery, New York in the west to Block Island Sound in the east, encompassing the region 73.8 °W - 72.01 °W and 40.74 °N - 41.4 °N. The grid has 100 increments in the east-west direction and 37 increments in the north-south direction, for a total of 3700 grid cells for each of seven vertical levels. The horizontal grid configuration with contours of water depth with respect to mean sea level is shown in Figure 4.1 for Long Island and Block Island Sounds. The nautical charts listed in Table 4.1 were used to develop representative grid cell depths with respect to mean low water. Subsequent adjustments were made to adjust the grid cell depths to the mean sea level. The average mid-Sound water depth with respect to mean sea level is on the order of 20 meters, with the deepest section, approximately 72 meters, occuring near The Race.

The vertical level discretization is presented in Table 4.2. More resolution is provided near the top and bottom of the water column in order to represent the surface and bottom boundary layers, respectively. Model water level boundary mean sea levels with respect to the 1929 National Geodetic Vertical Datum (NGVD) and with respect to the 1988 North American Vertical Datum (NAVD) are shown in Table 4.3 and Table 4.4, respectively. Relative to NGVD the difference between The Battery, NY and Vail Beach, RI is 88 mm, with The Battery, NY mean level standing higher. With respect to NAVD the corresponding difference is reduced by 52 mm. Since no long term water level measurement are available at Vail Beach, RI, table values at this station are assumed to be half way between the Montauk Point, NY and Point Judith, RI values. Note the cross Block Island Sound water level difference is 28 mm with respect to NGVD and 22 mm with respect to NAVD, with Montauk Point, NY standing higher than Point Judith, RI. Also given in Table 4.4 are the offsets to the mean sea levels with respect to NAVD used in the final eighteen month simulations. These offsets were determined in order to meet East River nontidal flux targets set by the USEPA in conjunction with NOAA/NOS.

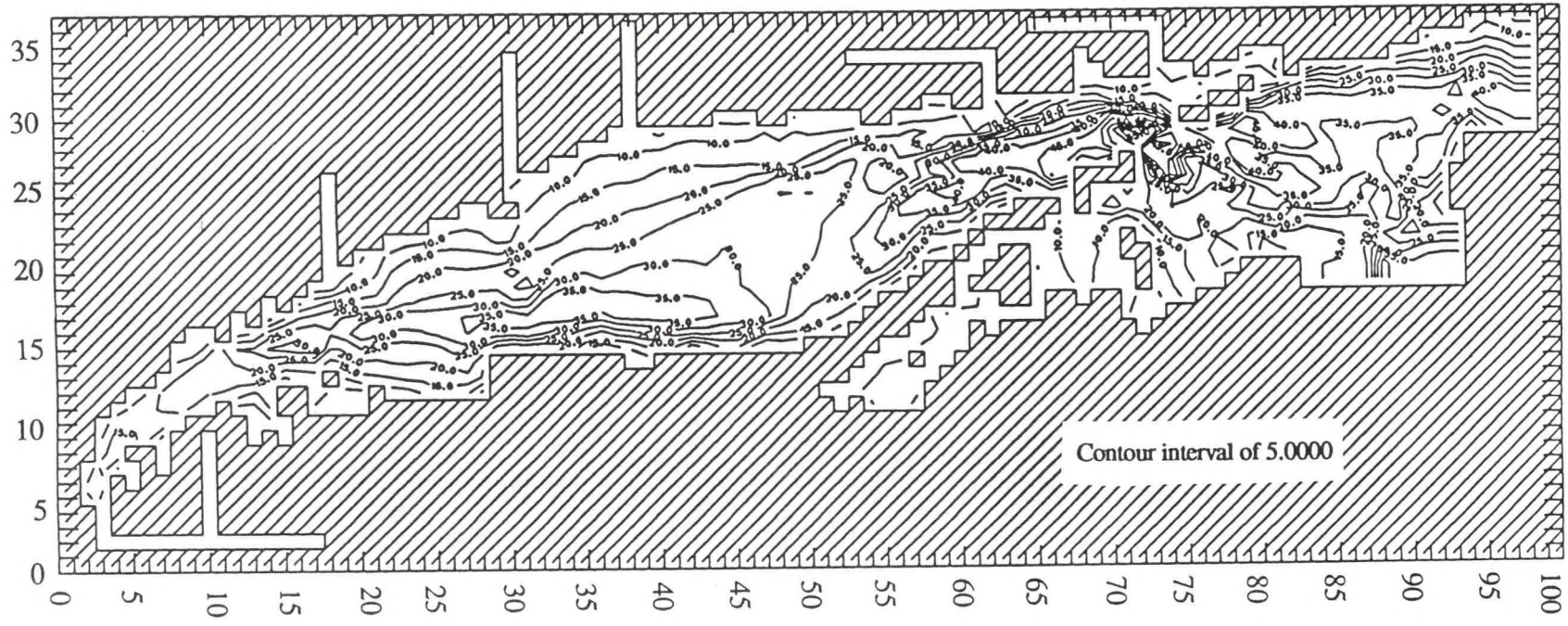

Figure 4.1. Long Island Sound Hydrodynamic Model Horizontal Grid with Contours of Water Depth (m MSL)

Table 4.1. Long Island Sound Model Grid Nautical Charts

	Nautical Chart No.	Scale	Title
Sound	13205	1:80000	Block Island Sound and Approaches
	12354	1:80000	Long Island Sound Eastern Part
	12363	1:80000	Long Island Sound Western Part
Rivers			
	12375	1:20000	Connecticut River
	12377	1:20000	Long Island Sound to Connecticut River Deep River to Badkin Rock
	12370	1:20000	North Shore of Long Island Sound : Housatonic River and Milford Harbor
	12371	1:20000	New Haven Harbor
	12368	1:20000	North Shore of Long Island Sound : Sherwood Point to Stamford Harbor
	12372	1:20000	Watch Hill to New Haven Harbor Pages A and B

Table 4.2. Vertical Discretization

Level K	σ_k	$\Delta\sigma_k$
1	0	-.1
2	-.1	.1
3	-.2	.2
4	-.4	.2
5	-.6	.2
6	-.8	.1
7	-.9	.1
8	-1.	-

Table 4.3. Mean Sea Level (MSL) 1929 National Geodetic Vertical Datum (NGVD) Differences Over Long Island and Block Island Sounds

Station No.	Name	Difference MSL - NGVD (m)
845-5083	Point Judith, RI	.111
845-9449	Vail Beach, RI	.125
851-0321	Montauk Point, NY	.139
851-8903	Spuyten Duyvil, NY	.262
851-8750	The Battery, NY	.213

Table 4.4. Mean Sea Level (MSL) 1988 North American Vertical Datum (NAVD) Differences Over Long Island and Block Island Sounds

Station No.	Name	Difference MSL - NAVD (m)	Datum Offset (cm)
845-5083	Point Judith, RI	-.169	6.7
845-9449	Vail Beach, RI	-.158	6.7
851-0321	Montauk Point, NY	-.147	6.7
851-8903	Spuyten Duyvil, NY	-.058	-0.4
851-8750	The Battery, NY	-.122	0.0

The Norwalk, Housatonic, Quinnipiac and Mill, Connecticut, and Thames River systems in Connecticut and the East and Harlem Rivers in New York were specially defined in terms of water depth and grid cell widths as shown in Tables 4.5 and 4.6, respectively. Both cell dimensions, Δx and Δy, are adjusted in river bends. River system cell width and depths were

Table 4.5. State of Connecticut River Geometries

Norwalk River

I,J	Depth (m)	Width (m)	Direction
18,19	8.85	2032	x
18,20	3.66	2032	x
18,21	3.05	152	x
18,22	3.05	152	x
18,23	3.05	152	x
18,24	3.05	152	x
18,25	3.05	152	x
18,26	3.05	152	x

Housatonic River

I,J	Depth (m)	Width (m)	Direction
30,25	6.33	2032	x
30,26	3.05	274	x
30,27	2.74	305	x
30,28	2.74	335	x
30,29	2.74	457	x
30,30	2.74	274	x
30,31	2.13	229	x
30,32	2.13	244	x
30,33	6.10	274	x
30,34	3.05	229	x

Quinnipiac and Mill Rivers

I,J	Depth (m)	Width (m)	Direction
38,31	5.22	2032	x
38,32	3.05	305	x
38,33	3.05	305	x
38,34	3.05	305	x
38,35	3.05	305	x
38,36	3.05	305	x

Table 4.5. (Continued) State of Connecticut River Geometries

Connecticut River

I,J	Depth (m)	Width (m)	Direction
62,31	6.13	2032	x
62,32	2.13	1372	x
62,33	3.05	914	x
62,34	4.57	762	x,y
61,34	3.66	610	y
60,34	2.44	457	y
59,34	6.10	305	y
58,34	4.27	914	y
57,34	9.14	305	y
56,34	3.05	853	y
55,34	5.49	335	y
54,34	6.10	305	y
53,34	4.57	366	y

Thames River

I,J	Depth (m)	Width (m)	Direction
73,33	10.4	2032	x
73,34	6.71	1372	x
73,35	7.62	1036	x
73,36	6.71	914	x,y
72,36	9.14	457	y
71,36	3.66	549	y
70,36	3.66	610	y
69,36	2.44	610	y
68,36	2.74	457	y
67,36	2.74	305	y
66,36	3.66	305	y
65,36	6.10	152	y

Table 4.6. State of New York River Geometries

East River

I,J	Depth (m)	Width (m)	Direction
3,4	21.8	914	x
3,3	13.6	1118	x
3,2	14.8	2032	x,y
4,2	11.4	914	y
5,2	13.5	610	y
6,2	14.7	711	y
7,2	15.5	508	y
8,2	16.6	508	y
9,2	16.0	406	y
10,2	14.7	2032	x,y
11,2	13.5	711	y
12,2	12.8	1016	y
13,2	13.1	508	y
14,2	13.4	508	y
15,2	14.0	508	y

Harlem River

I,J	Depth (m)	Width (m)	Direction
10,3	6.8	188	x
10,4	6.8	130	x
10,5	6.8	130	x
10,6	6.8	130	x
10,7	6.5	130	x
10,8	6.5	100	x
10,9	6.5	80	x
16,2	12.2	711	y

were determined to specify representative flow conveyance areas. Grid resolution is insufficient to represent the details of plume evolution within the river systems. The approach implemented inputs the freshwater inflow volumes to the Sound for each river system at the appropriate shoreline location.

4.2. Numerical Stability Conditions

Considering the stability condition of Equation (2.35) with H=72m, Δx=Δy= 2032m, $\bar{u}_{max}$ = 2 m/s, then C_t^E = 55 m/s and Δt_E^1 = 26.1 seconds. In both the initial astronomic tide and eighteen month long-term simulations, employ Δt = 30.0 seconds for a External Courant Number, $Cr_E = \Delta t/\Delta t_E$ = 1.15. In actuality, the factor of two times the gravity wave speed represents the worst case condition for gravity wave propagation in the direction of the grid cell diagonal. In the case of gravity wave propagation in the direction parallel to the grid cell sides, the factor becomes unity. In the Long Island Sound simulations, the gravity waves do not propagate truly diagonally and the Courant Number based on this condition exceeds unity.

The rotation limit, Δt_E^2, is evaluated in the following manner. The average latitude of the grid is 41.05 °N and by Equation (2.36), $\Delta t_E^2 = 10^4$ seconds. Thus, this rotation condition is clearly not limiting in this application and $\Delta t_E = \Delta t_E^1$.

For the internal mode stability condition of Equation (2.37), assuming a freshwater layer (1000 kg/m^3) over a layer of seawater (1025 kg/m^3), $\Delta\rho/\rho_o$ = .025 and U_{max} = 2 m/s, then C_t^I = 10.4 m/s and ΔT_I^2 = 138 seconds. For $\Delta x = \Delta y$ = 2032 m and $u_{max} = v_{max}$ = 1 m/s, and a grid cell Reynolds number of unity, based upon Equation (2.38) ΔT_I^2 = 254 seconds. In the vicinity of river bends, this limit is further reduced to approximately 200 seconds, but still $\Delta T_I = \Delta T_I^1$.

For the long-term eighteen month simulation, we employ ΔT = 150 seconds at a Internal Courant Number, Cr_I = 1.09. Analogous considerations hold for the direction of internal wave propagation allowing a Internal Courant Number greater than unity to be utilized. Note that a mode split (ratio of internal to external mode time steps) of 5:1 is used. For the September 1988 astronomic tide simulation, the relative density change over the vertical is much less than .025, and a 10:1 mode split is used.

4.3. Initial Condition Specification

To initiate computations, it is necessary to specify water surface elevation ($\eta^m_{i,j}$, $\eta^{m-1}_{i,j}$), vertically integrated velocity components $\left(\bar{u}^m_{ij}, \bar{u}^{m-1}_{ij}\right)$, two horizontal velocity components ($u^n_{i,j,k}$, $u^{n-1}_{i,j,k}$, $v^n_{i,j,k}$, $v^{n-1}_{i,j,k}$), salinity ($S^n_{i,j,k}$, $S^{n-1}_{i,j,k}$), temperature ($T^n_{i,j,k}$, $T^{n-1}_{i,j,k}$), turbulent kinetic energy $\left(q^{2^n}_{i,j,k}, q^{2^{n-1}}_{i,j,k}\right)$, product of turbulent kinetic energy and length scale

$\left(q^2\ell^n_{i,j,k},\ q^2\ell^{n-1}_{i,j,k}\right)$, the vertical mixing coefficient for momentum $\left(K^n_{m_{i,j,k}}\right)$, the vertical mixing coefficient for temperature/salinity $\left(K^n_{H_{i,j,k}}\right)$, and the vertical mixing coefficient $\left(K^n_{q_{i,j,k}}\right)$ for turbulence. The initial salinity and temperature fields are developed using more elaborate procedures as outlined below.

Water Surface Elevation, Velocity, and Turbulence Quantities

The following relations are employed to set initial conditions.

$$\eta^0_{ij} = \eta^{-1}_{ij} = 0 \quad (m) \ , \tag{4.1a}$$

$$\bar{u}^0_{ij} = \bar{u}^{-1}_{ij} = u^0_{i,j,k} = u^{-1}_{i,j,k} = 0 \quad (m/s) \ , \tag{4.1b}$$

$$q^{2\,0}_{i,j,k} = q^{2\,-1}_{i,j,k} = 1. \times 10^{-4} \quad (m^2/s^2) \ , \tag{4.1c}$$

$$q^2\ell^0_{i,j,k} = q^2\ell^{-1}_{i,j,k} = 1. \times 10^{-4} \quad (m^3/s^2) \ , \tag{4.1d}$$

$$\ell^0_{i,j,k} = \ell^{-1}_{i,j,k} = 1 \quad (m) \ , \tag{4.1e}$$

$$K^0_{m_{i,j,k}} = K^0_{H_{i,j,k}} = .2 \times 10^{-4} \quad (m^2/s) \ , \text{ and} \tag{4.1f}$$

$$K^0_{q_{i,j,k}} = .2\,\ell^0_{i,j,k}\sqrt{q^{2\,0}_{i,j,k}} = .2 \times 10^{-2} \quad (m^2/s) \ . \tag{4.1g}$$

Synthesis of Three-Dimensional Salinity and Temperature Fields: Principles

The synthesis of the three-dimensional salinity and temperature fields over the computational grid is desired for two reasons. First, it is necessary to initialize the computations with a complete set of salinity and temperature fields. The initial estimate should approximate in-situ synoptic conditions as closely as possible to minimize model spin-up time. If initial salinity and temperature fields were set to zero and prototype salinity and temperature conditions specified at river inflow points and along the open boundary, it might require several months of simulation to affect a reasonable salinity and temperature field over the complete computational domain. To eliminate this increased computational requirement, it is desireable to synthesize a representative initial state for both salinity and temperature. Secondly, since conductivity and temperature versus depth (CTD) measurements are available over the eighteen month simulation period, it is possible to use the same technique to synthesize salinity and temperature fields at the initial time and at regular intervals (beginning of each month) over the computational grid. This allows a comparison of model generated salinity and temperature fields with fields interpolated from observational data. Favorable comparison tends to enhance the credibility of both the model performance and the ability to construct entire fields from limited sets of observations.

To develop the method, the set of CTD casts at unequally-spaced times represented in Equation

(4.2) below is reformatted by subtracting the surface value from the value at each cast depth , Equation (4.3) below. At the first day of each month over the period, April 1988 - September 1989, appropriate reformatted casts are assumed to represent the vertical stratification.
The functional forms presented in Equation (4.4) are assumed to represent the surface conditions. These functional forms are closed form in time, t, and therefore can be used to estimate the surface conditions at any given time. A synoptic set of surface conditions is developed and the reformatted casts are added to the surface condition to determine the complete vertical profile. Thus, a synoptic set of temperature and salinity profiles are achieved. To develop salinity and temperature fields over the complete grid, an inverse squared distance interpolation is performed over a set of non-overlapping patches encompassing the complete horizontal grid. A special vertical interpolation based on grid cell depth and not on the sigma level is performed. With this outline in mind, the complete method in terms of first principles is next presented.

Consider the set of CTD casts, $\mathcal{F}$, encompassing the entire Long Island Sound region to be represented in the following manner:

$$\mathcal{F} = \{d_{ij}, t_j, S_{ij}(d_{ij}, t_j), T_{ij}(d_{ij}, t_j)\} \quad i = 0, m_j \quad j = 1, L \tag{4.2}$$

where

d_{ij} ≡ cast depth i at CTD station j,
t_j ≡ time of the cast at station j,
S_{ij} ≡ cast salinity (psu) at depth i at CTD station j,
T_{ij} ≡ cast temperature (°C) at depth i at CTD station j,
m_j ≡ number of depths at station j, and
L ≡ total number of CTD stations.

Let $i = 0$ correspond to the water surface and for ease of notation set $S_{0j}(d_{oj}, t_j) = S_{oj}(t_j)$. We represent the vertical structure in the set of casts in the following alternate form; i.e., by the difference between local salinity and surface salinity.

$$\Delta S_{ij}(t_j) = S_{ij}(d_{ij}, t_j) - S_{0j}(t_j) \tag{4.3a}$$

$$\Delta T_{ij}(t_j) = T_{ij}(d_{ij}, t_j) - T_{0j}(t_j) \quad . \tag{4.3b}$$

Since the set $\{t_j\}$ is not synoptic ;i.e., $t_1 \neq t_2, \ldots, t_{L-1} \neq t_L$, it is necessary to develop a method for adjusting the casts to a common time point, which is considered sufficiently close to each cast time, t_j, such that the vertical structure in Equation (4.3) is valid at time t. With this in mind, assume that the following functional forms hold for salinity and temperature.

$$\check{S}_{ij}(d_{ij}, t) = \check{S}_{0j}(t) + \Delta S_{ij}(t_j) \tag{4.4a}$$
$$\check{T}_{ij}(d_{ij}, t) = \check{T}_{0j}(t) + \Delta T_{ij}(t_j) \tag{4.4b}$$

with

$$\check{S}_{0j}(t) = \bar{S}_j + A_j^S \cos\left(a_{M_2} t + (V_0 + u)_{M_2} - \phi_j^s\right)$$

$$\check{T}_{0j}(t) = \bar{T}_j + A_j^T \cos\left(s\,t + (V_0 + u)_T - \phi_j^T\right)$$

where

$\check{S}_{ij}(t)$	≡	Salinity at depth i at CTD station j at time t,
$\check{T}_{ij}(t)$	≡	Temperature at depth i at CTD station j at time t,
$\check{S}_{0_j}(t)$	≡	Functional form for surface salinity,
$\check{T}_{0_j}(t)$	≡	Functional form for surface temperature,
$\bar{S}_j$	≡	Estimate of mean tidal cycle value of surface salinity,
$\bar{T}_j$	≡	Estimate of mean solar day value of surface temperature,
A_j^S	≡	Mean amplitude of surface salinity over a tidal cycle,
A_j^T	≡	Mean amplitude of surface temperature over a solar day,
a_{M_2}	≡	M_2 tidal constituent speed (28.9841 °/hr),
s	≡	Solar angular velocity (15 °/hr),
$(V_0+u)_{M_2}$	≡	Equilibrium argument for the M_2 tidal constituent,
$(V_0+u)_T$	≡	Equilibrium argument for temperature (135 °),
ϕ_j^S	≡	M2 constituent tidal phase at the nearest water level station, and
ϕ_j^T	≡	Hour angle of maximum temperature.

Observe that by assuming ϕ^S_j equal to the M_2 phase at station j, found from the nearest tidal elevation station, the salinity is a maximum at high tide and minimum at low tide. Note that ϕ_j^T is set to zero degrees so that at hour 15 the temperature is a maximum and at hour 3 the temperature is a minimum. Therefore, given a t in Julian days (corresponding to the set of times April 1, 1998, hour zero through October 1, 1989, hour zero at monthly intervals), it is possible to generate a synoptic set of CTD-type data.

To develop the full three-dimensional fields, the following spatial interpolation is performed over a set of rectangular patches in the horizontal. Each horizontal patch is defined in terms of a lower and upper index value in each horizontal coordinate, $i_1 \leq i \leq i_2$ and $j_1 \leq j \leq j_2$, respectively. The four patch grid points (ipt_n, jpt_n), $n=1,4$ are given as

$(ipt_1,jpt_1) = (i_1,j_1)$, $(ipt_2,jpt_2) = (i_2,j_1)$, $(ipt_3,jpt_3) = (i_2,j_2)$, and $(ipt_4,jpt_4) = (i_1,j_2)$. The set of patches is complete and non-overlapping. In each patch, the following inverse squared distance spatial interpolation procedure is employed by assigning a synoptic CTD-type cast to each of the four corners of the patch; e.g., for $n = 1, \ldots 4$, $hin(nd_n,n)$, $T(nd_n,n)$ and $S(nd_n,n)$ represent arrays containing the nd_n cast depths and corresponding synoptic temperature and salinity. Computational steps for each patch are itemized below:

I. a. Set $S_{i,j,k} = T_{i,j,k} = 0$ in land cells, $i_1 \le i \le i_2$ $j_1 \le j \le j_2$, $k = 1, KB-1$.

b. In water cells, compute sigma level k (Equation (2.24)) interpolation depth $di_k = -\sigma L_k h_{i,j}$ and set $nint = 0$.

II. a. Next consider each of the four grid points defining the patch (ipt_n,jpt_n) n = 1, ... 4.

If the grid cell still water depth, $h_{ipt_n,jpt_n} > di_k$ or the cast depth $hin(nd_n,n) \ge di_k$,

then $nint = nint + 1$,
$T(nint) = LI(\, di_k, hin(nd_n,n), T(nd_n,n)\,)$,
$S(nint) = LI(\, di_k, hin(nd_n,n), S(nd_n,n)\,)$,
where LI consists of a linear interpolation operator; i.e., $T(nint)$ at depth di_k is linearly interpolated from $hin(nd_n,n)$, and $S(nd_n,n)$ array values.

b. If there are no interpolation points, then $nint = 0$ and $k > 1$. Then assume
$T_{i,j,k} = T_{i,j,k-1}$ and
$S_{i,j,k} = S_{i,j,k-1}$,
which extends the last interpolation value at (i,j,k-1) to the next layer below (i,j,k).

c. If $nint \neq 0$, then an inverse squared distance spatial interpolation of the following form is applied.

$$dy_n = alat_{i,j} - alat_{ipt_n,jpt_n} \,, \tag{4.5a}$$

$$dx_n = \frac{\left(alon_{i,j} - alon_{ipt_n,jpt_n}\right)}{\cos\left(\overline{alat_n}\right)} \,, \tag{4.5b}$$

$$\overline{alat_n} = .5\left(alat_{i,j} + alat_{ipt_n,jpt_n}\right) \,, \tag{4.5c}$$

$$d_n = dx_n^2 + dy_n^2 \,, \tag{4.5d}$$

$$d_T = \sum_{n=1}^{nint} d_n \,, \quad \omega_n = \frac{d_n}{d_T} \,, \tag{4.5e}$$

$$T_{i,j,k} = \sum_{n=1}^{nint} \omega_n T_n \,, \text{ and } \quad S_{i,j,k} = \sum_{n=1}^{nint} \omega_n S_n \,. \tag{4.5f}$$

Note that in utilizing the above procedures, some judgement is required in first setting up the set of patches, second in assigning synoptic CTD-type casts to each of the four corners of a patch, and third in extending depths of synoptic CTD-type casts at particular locations such as at the head of tide of rivers. Patch corners may be on land and do no have to correspond to observation points. As a result, the development of the initial and synthesized salinity and temperature fields using these techniques is an iterative process.

Synthesis of Three-Dimensional Salinity and Temperature Fields: Implementation

Prior to long term simulation, a one month (September 1988) astronomic tide simulation, including density effects, was performed. The above procedures were utilized to provide the initial conditions for the salinity and temperature fields. Simulation over the eighteen month period, April 1988 -September 1989, was performed in two month intervals. After the initial two month simulation, subsequent two month simulations were restarted. As a result, it was necesary to develop initial conditions for the salinity and temperature fields on April 1, 1988 to initiate the eighteen month simulation.

Procedures outlined above were used on the CTD data collected by the State University of New York (SUNY) and the University of Connecticut (UCONN). Based upon review of the longitudinal profile of salinity averaged over September 1988, the mean salinity at the stations shown in Figure 4.2 was well represented by a piecewise linear function of distance from station P11 at The Battery, NY.

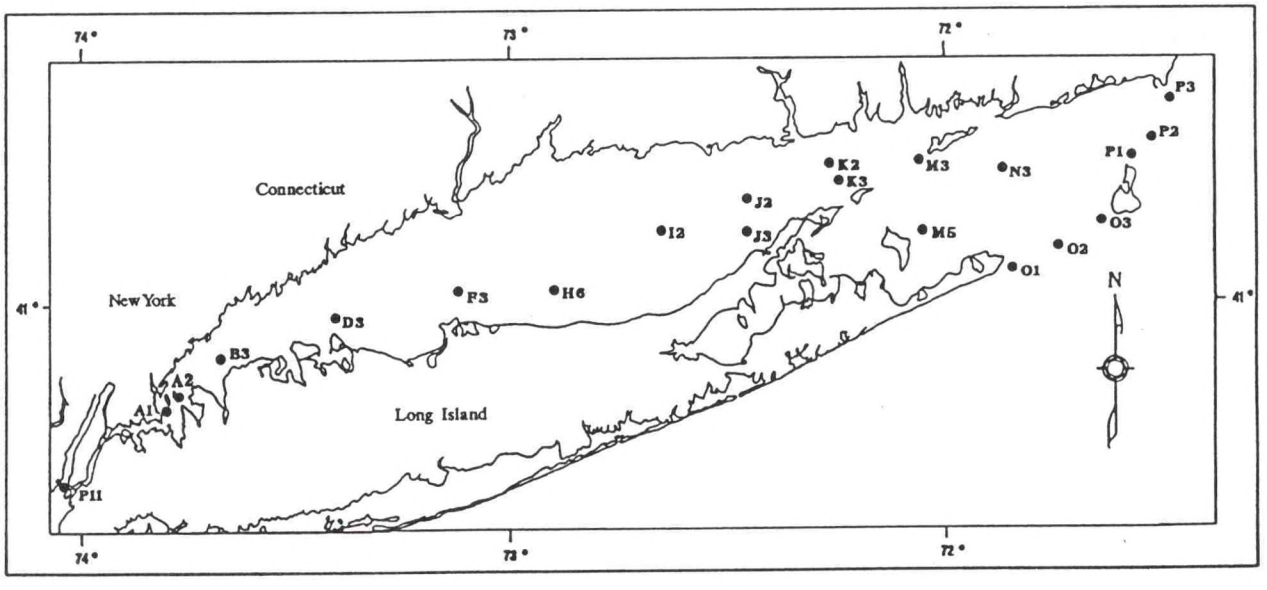

Figure 4.2. Long Island Sound Interpolation, CTD Stations

The total difference in mean salinity between the the Block Island Sound northern boundary and The Battery, ΔS, was distributed equally among the following three sectors designated by station number. Sector 1 covered locations from station P11 to station B3, sector 2 from stations B3 to K3, and sector 3 from stations K3 to P3, respectively.

Based upon review of the average longitudinal temperature profile for September 1988, the total difference in mean temperature between stations P11 and P3, ΔT, was well represented by a one piece linear function of distance between these stations. These functional forms allowed the adjustment factors shown in Table 4.6 to be determined. The product of these adjustment factors and $\Delta S/3$ or ΔT were added to and subtracted from station P11 values in the cases of salinity and temperature, respectively. Mean amplitudes $\bar{A}_j^S = 0.3$ psu and $\bar{A}_j^T = 0.4$ C as defined in Equation (4.4) were used. As defined in Equation (4.4), M_2 phase angles, ϕ_j^S are given in Table 4.7, while $\phi_j^T = 0$ was assumed for all stations.

Table 4.7. Interpolation Station: Salinity and Temperature Adjustment Factors and M2 Salinity Phase Angles, ϕ_j^S

Station	Salinity Adjustment Factor	M_2 Phase (°)	Temperature Adjustment Factor
P11	0.	238.	0.
A1	0.39	332.	0.06
A2	0.14	332.	0.03
B3	0.47	329.	0.07
D3	0.16	335.	0.1
F3	0.19	323.	0.1
H6	0.15	327.	0.08
I2	0.2	327.	0.11
J3	0.13	310.	0.07
K3	0.16	290.	0.08
L1	0.15	291.	0.05
M5	0.05	270.	0.02
N3	0.30	247.	0.07
O1	0.03	214.	0.07
O3	0.26	216.	0.08
P1	0.1	219.	0.03
P3	0.11	218.	0.04
Totals	3.0		1.0

On September 1 1988, the mean salinity and temperature at P11 were 24.0 psu and 21.5 C,

respectively. The mean salinity and temperature conditions at P3 were 32.0 psu and 18.9 C, respectively, resulting in ΔT = 2.6 °C and ΔS = 8 psu, respectively. Using the above adjustment factors, the mean surface salinity, $\bar{S}_j$, and temperature, $\bar{T}_j$, given in Equation (4.4) at the intermediate station locations were determined as shown in Table 4.8

Table 4.8. Mean Surface Salinity and Temperature for September 1, 1988

Station	Temperature °C	Salinity (psu)
P11	21.50	24.00
A1	21.34	25.04
A2	21.26	25.38
B3	21.08	26.64
D3	20.82	27.07
F3	20.56	27.57
H6	20.35	27.97
I2	20.06	28.50
J3	19.88	28.84
K3	19.67	29.27
L1	19.54	29.67
M5	19.49	29.83
N3	19.31	30.64
O1	19.28	30.71
O3	19.07	31.44
P1	18.99	31.70
P3	18.90	32.00

The synoptic CTD cast number and dates of the original CTD casts used in the salinity and temperature field interpolation procedure are given in Table 4.9. In addition to these seventeen casts, ten casts were developed to provide for interpolation in the five Connecticut river sections. Cast numbers 18, 20, 22, 24, and 26 were constructed to represent conditions at the upstream river boundary. Temperature and salinity were assumed to be vertically uniform at 20 °C and 0 psu, respectively. Cast numbers 19, 21, 23, 25, and 27 were constructed to represent conditions at the river mouth and were considered to be identical to casts 11, 9, 7, 6, and 5, respectively. The complete interpolation was performed over the twenty separate patches listed in Table 4.9. An additional patch not shown in Table 4.9 covering the Harlem River ($i_1 = i_2 = 10$, $j_1 = 3$, $j_2 = 10$) was also employed. The first four columns list the grid (i,j) coordinates defining the patch, while the last four columns refer to the CTD cast numbers (Table 4.8) assigned to each of the four corners of the patch. Similar considerations hold for April 1, 1988 initial salinity and temperature field determination. In this case however, the longitudinal temperature profile was not a simple linear function of distance and had to be constructed on a station by station basis. The salinity at the open ocean boundary was reduced from 32. psu to 31. psu. Twenty five CTD casts were employed in the spatial interpolation procedures.

Table 4.9. September 1988 Initial Salinity and Temperature Fields

Part a. CTD Cast Numbers and Dates

CTD Cast Number	Station	Cast Dates Salinity	Cast Dates Temperature
1	P11	8/15/88	9/13/88
2	A1	8/15/88	9/13/88
3	A2	8/15/88	8/29/88
4	B3	8/15/88	8/29/88
5	D3	8/16/88	8/29/88
6	F3	8/11/88	8/29/88
7	H6	8/17/88	8/29/88
8	I2	8/18/88	9/1/88
9	J3	9/8/88	9/8/88
10	K3	9/7/88	9/7/88
11	L1	9/7/88	9/7/88
12	M5	9/7/88	9/7/88
13	N3	9/6/88	9/6/88
14	O1	9/6/88	9/6/88
15	O3	9/6/88	9/6/88
16	P1	9/6/88	9/6/88
17	P3	9/6/88	9/6/88

Part b. Interpolation Patch Definitions

	Grid Cell I and J Upper and Lower Indicies				CTD Cast Number Points			
Patch No.	i_1	i_2	j_1	j_2	1	2	3	4
1	2	20	2	3	2	1	1	2
2	2	3	3	5	2	2	3	3
3	2	8	6	37	3	4	4	3
4	8	18	3	37	4	5	5	4
5	18	28	3	37	5	6	6	5
6	28	38	3	37	6	7	7	6
7	38	49	3	37	7	8	8	7
8	49	58	3	37	8	9	9	8
9	58	65	3	37	9	10	10	9
10	65	70	3	37	10	11	11	10
11	70	74	3	37	11	12	12	11
12	74	82	3	37	12	13	13	12
13	82	84	3	37	13	14	14	13
14	84	94	3	37	14	15	16	13
15	94	100	3	37	16	17	17	16
16	26	30	25	30	25	25	24	24
17	33	38	30	32	23	23	22	22
18	53	62	32	34	21	21	20	20
19	65	73	36	36	19	19	18	18
20	73	73	32	36	19	19	18	18

4.4. Boundary Condition Specification

To apply the internal and the external mode equation sets of Section 2, a set of boundary conditions must be properly posed. Let us consider the complete boundary, Ω, to be defined as follows:

$$\Omega = \Omega_{\ell c} + \Omega_{\ell o} + \Omega_{\ell f} + \Omega_S + \Omega_b \tag{4.6}$$

where

$\Omega_{\ell c}$ $\equiv$ closed lateral boundary,
$\Omega_{\ell f}$ $\equiv$ flow lateral boundary,
$\Omega_{\ell o}$ $\equiv$ open lateral boundary,
Ω_S $\equiv$ surface boundary, and
Ω_b $\equiv$ bottom boundary.

It is necessary to consider the above five boundary conditions for the three-dimensional (internal-mode) equation set as well as the vertically integrated (external-mode) equation set. We do so in turn below.

Internal-Mode

We consider the full equation set given in Table 2.1; namely, [1] Continuity Equation, [2] x'-Momentum Equation, [3] y'-Momentum Equation, [4] Temperature Equation, [5] Salinity Equation, [6] Turbulent Kinetic Energy Equation, and [7] Turbulent Macroscale Equation.

In considering boundary conditions, we let n' correspond to the horizontal coordinate in the direction normal to the boundary and o' correspond to the perpendicular horizontal coordinate direction, respectively. All boundary conditions are itemized separately in tables. Note the numbers in square brackets next to the left margin in these tables refer to the equation numbers in Table 2.1. Closed lateral boundary conditions, $\Omega_{\ell c}$, are itemized in Table 4.10 and constitute all land/water lateral boundaries. It is not necessary to supply any external forcing data to affect these boundary conditions.

Lateral flow boundary conditions, $\Omega_{\ell f}$, are listed in Table 4.11. We consider the specification of river inflow conditions by assuming that the flow is uni-directional into the estuary at surface speed, U_f, at the inflow point, which is above the head of tide. It is necessary to supply volumetric flow rate, $Q(t)$, salinity, $S_r(t)$, and temperature, $T_r(t)$, time series for each river as inflow specifications. The procedures used are outlined in turn below.

First, note that $\int_{-1}^{0} u_{n'} d\sigma = \int_{-1}^{0} U_f(1-\sigma^2) d\sigma = \frac{2U_f}{3}$. For a volumetric flow rate, $Q(t)$, note that $\frac{2}{3} U_f H(\Delta o') = Q(t)$, and since above the head of tide $H = h$,

Table 4.10. Closed Lateral Boundary ($\Omega_{\ell c}$) Conditions

Equation	Condition
[1,2,3,4,5,6,7]	$u = 0$ *if* $n' = x'$ $v = 0$ *if* $n' = y'$
[4]	$Q_{n'T} = 0$
[5]	$Q_{n'S} = 0$
[6]	$Q_{n'q^2} = 0$
[7]	$Q_{n'q^2\ell} = 0$

$U_f = \frac{3}{2}\frac{Q(t)}{h\Delta o'}$. In the numerical integration over seven vertical levels a factor of 1.4390 results rather than 1.5, which would be achieved for an infinite number of vertical levels.

Table 4.11. Flow Lateral Boundary ($\Omega_{\ell f}$) Conditions

Equation	Condition
[1,2,3,4,5,6,7]	$u_{n'} = U_f(1 - \sigma^2)$ $u_{o'} = 0$
[4]	$T = T_r(t)$
[5]	$S = S_r(t)$
[6]	$\frac{\partial(q^2)}{\partial n'} = 0$
[7]	$\frac{\partial(q^2 l)}{\partial n'} = 0$

Average daily streamflows were obtained from the United States Geological Survey (USGS), Water Resources Data for Connecticut (1988, 1989), for the five major river systems in Connecticut given in Table 4.12 over the period April 1988 - September 1989. The combined drainage area of these five systems comprises 14,976 square miles or approximately 91 percent

of the total Long Island Sound drainage area of 16,500 square miles. In order to estimate the total flow in each river system, individual river flows were summed and multiplied by the ratio of the gaged drainage area and the system drainage area (shown in parentheses following the system name) raised to the 0.87 power based on USGS guidance (Weiss, 1988). The above procedure was used separately for the Quinnipiac and Mill rivers. A linear temporal interpolation procedure was used to determine inflow in cubic feet per second at external mode time steps at locations shown in Table 4.12. All flow rates are converted to velocity in meters per second using the still water depth and stream flow width. Maximum average daily flows for the period of record are given in the last column of Table 4.12. None of these maximums occurred during the 1988 - 1989 period.

Mean surface salinity and temperature were specified at the head of tide at monthly intervals. Well-mixed conditions were assumed so that salinity and temperature were considered vertically uniform. A linear temporal interpolation technique in time was used to specify conditions at each internal-mode time step.

Average daily streamflows for the five New York streams given in Table 4.13 were obtained from the USGS, Water Resource Data for New York (1988, 1989). Maximum average daily flows are given for the period of record. None of these maximums occurred during the 1988 - 1989 period. Since these streamflows are generally much smaller in magnitude than the Connecticut rivers, they were treated as point sources to the surface model layer as discussed in Section 3. Salinity was considered zero and inflow temperature set equal to the value of the temperature in the input cell's surface layer.

Sewage treatment plant inflows to the East River shown in Table 4.14 were considered time invariant point sources to the bottom model layer. Salinity was considered zero and inflow temperature was set equal to the value of the temperatue in the input cell bottom layer.

Combined sewer overflows (CSOs) for the seven signals in Table 4.15 were provided by EPA on a monthly interval based upon rainfall-runoff analyses. These flow signals represent average flowrates based on fractions of CSOs by the counties shown, and were distributed among the appropriate grid cells by multiplying by the flow factors listed in the last column of Table 4.15. The flows were considered surface layer point sources. Salinity was zero and temperature was set equal to the value of the temperature in the input cell's surface layer.

Open lateral boundary conditions are listed in Table 4.16. Water surface elevations specified for the five tidal boundary signals given in Table 4.17 are employed at locations shown in Figure 4.3. Local Standard Time (which corresponds here to Eastern Standard Time) is used as the time reference for all water surface elevation data. We used the specification of a tidal elevation condition determined from a harmonic analysis of tide gage data. The prediction equation of Shureman (1958) is employed for each boundary elevation signal, I, as follows

$$h_I(t) = H_0^I + \sum_{j=1}^{37} f_j H_{jI} \cos\left(a_j t + \left(V_0 + u\right)_j^G - \kappa'_{jI}\right) \qquad (4.7)$$

Table 4.12. Major Connecticut River Systems Draining into Long Island Sound

System I: Connecticut River (11,263 mi^2) Model Indicies (55,34)

Station Name	Drainage Area (mi^2)	USGS Gage No.	Max Average Daily Flow (cfs)
Connecticut River at Thompsonville, CT	9660	01184000	282,000
Farmington River at Tariffville, CT	577	01189995	29,900
Hockanum River near East Hartford, CT	73.4	01192500	5,160
Salmon River near East Hampton, CT	100	01193500	18,500
Total	10,410.4		

System II: Housatonic River (1946 mi^2) Model Indicies (28,30)

Station Name	Drainage Area (mi^2)	USGS Gage No.	Max Average Daily Flow (cfs)
Housatonic River at Stevenson, CT	1544	01205500	75,800
Naugatuck River at Beacon Falls, CT	260	01203500	106,000
Total	1804		

System III: Norwalk River (64.2 mi^2) Model Indicies (18,25)

Station Name	Drainage Area (mi^2)	USGS Gage No.	Max Average Daily Flow (cfs)
Norwalk River at South Wilton, CT	30	01209700	2,890

System IV: Thames River (1478 mi^2) Model Indicies (67,36)

Station Name	Drainage Area (mi^2)	USGS Gage No.	Max Average Daily Flow (cfs)
Quinabaug River at Jewett City, CT	713	01127000	40,700
Yantic River at Yantic, CT	89.3	01127500	13,500
Shetucket River near Williamantic, CT	404	01122500	52,200
Little River near Hanover, CT	30	01123000	2,450
Total	1236.3		

System V: Quinnipiac and Mill Rivers (186 mi^2, 38.5mi^2) Model Indicies (35,32)

Station Name	Drainage Area (mi^2)	USGS Gage No.	Max Average Daily Flow (cfs)
Quinnipiac River at Wallingford, CT	115	01196500	8,200
Mill River near Hamden, CT	24.5	01196620	5,580
Total	139.5		

Table 4.13. New York Streams Draining into Long Island Sound

Station Name	Drainage Area (mi^2)	Max Average Gage Number	Indices Daily flow (cfs)	(I,J)
Blind Brook, Rye	9.20	01300000	2320.	(6, 12)
Bronx River, Bronxville	26.5	01302000	2500.	(6, 2)
Beaver Swamp, Mamaroneck	4.7	01300500	288.	(4, 11)
Mamaroneck River, Mamaroneck	23.4	01301000	3700.	(5, 12)
Hutchinson River, Pelham	5.8	01301500	526.	(2, 7)

Table 4.14. Sewage Treatment Plant Inputs to the East River

Location	Average Daily Flow (cfs)	Indicies (I,J)
Red Hook	68.5	(14, 2)
Newtown Creek	529.9	(13, 2)
Wards Island	341.1	(10, 2)
Bowery Bay	224.7	(8, 2)
Hunts Point	217.2	(7, 2)
Tallmans Island	100.0	(5, 2)

Table 4.15. Combined Sewer Overflow Inputs to the East River and Western Long Island Sound

Signal	Originating Counties	Model Indicies (I,J)	Flow Factor
1	1/2 Manhattan, 1/2 Kings	(15, 2)	1.
2	1/2 Manhattan, 1/2 Queens	(12, 2)	.5
2	"	(11, 2)	.5
3	1/3 Bronx, 2/3 Queens	(9, 2)	1.
4	1/2 Bronx, 1/2 Queens	(4, 2)	1.
5	1/2 Westchester, 1/2 Nassau	(2, 3)	.5
5	"	(3, 3)	.5
6	1/2 Westchester, 1/2 Nassau	(2, 5)	.25
6	"	(2, 6)	.25
6	"	(3, 5)	.25
6	"	(3, 6)	.25
7	1/2 Westchester, 1/2 Nassau	(2, 7)	.166
7	"	(3, 9)	.166
7	1/2 Westchester, 1/2 Nassau	(3, 10)	.166
7	"	(4, 7)	.166
7	"	(4, 8)	.166
7	"	(5, 9)	.166

Table 4.16. Open Lateral Boundary ($\Omega_{\ell o}$) Conditions

Equation	Condition
[1,2,3]	$\eta = \eta_a(t)$
[1,2,3,4,5,6,7]	$u_o' = 0$
[1,2,3,4,5,6,7]	$\frac{\partial u_n'}{\partial t} + c\frac{\partial u_n'}{\partial n'} = 0$
[4]	$T_{n'} = T_a(t) \qquad u_n' < 0$
	$Q_{x'T} = Q_{y'T} = 0; \quad \frac{\partial (Hu_{o'}T)}{\partial o'} = 0 \qquad u_n' > 0$
[5]	$S_{n'} = S_a(t) \qquad u_n' < 0$
	$Q_{x'S} = Q_{y'S} = 0; \quad \frac{\partial (Hu_{o'}S)}{\partial o'} = 0 \qquad u_n' > 0$
[6]	$\frac{\partial (q^2)}{\partial n'} = 0$
[7]	$\frac{\partial (q^2 l)}{\partial \eta'} = 0$

where

$\eta_a(t)$ ≡ specified water surface elevation with respect to model datum,
c ≡ gravity wave speed,
$T_a(t)$ ≡ specified salinity time series,
$S_a(t)$ ≡ specified temperature time series, and
$Q_{x'T}$, $Q_{x'S}$ are as defined in Table 2.2 in Equation (S.4).

where

$h_I\ (t)$ ≡ predicted elevation at time t for boundary signal I (ft),
f_j ≡ node factor for constituent j for the prediction period,
$(V_0 + u)_j^G$ ≡ Greenwich equilibrium argument for constituent j for the prediction period (°),
a_j ≡ constituent j speed (°/hr),

H_{jI} ≡ amplitude of constituent j (ft) for boundary signal I,
κ'_{jI} ≡ phase of constituent j (°) for boundary signal I,
t ≡ local Standard Time (hrs) from January 1, 1988, and
H^I_o ≡ mean water level relative to the model datum (ft).

The above equation is used to reconstruct the predicted water level based upon the set of harmonic constants (H_{jI}, κ'_{jI}). Since distinct sets of vertical datums and harmonic constants have been employed in different study components, these are discussed individually.
The total water level for each boundary signal is given by the following relationship.

$$ht_I(t) = h_I(t) + \alpha r_I(t) \tag{4.8}$$

where

$ht_I(t)$ ≡ Total elevation at time t for boundary signal I,
$h_I(t)$ ≡ Predicted elevation at time t for boundary signal I,
α ≡ Switch equal to either zero or one for boundary signal I, and
$r_I(t)$ ≡ Residual elevation at time t for boundary signal I.

Note that if $\alpha = 0$, the total elevation is equal to the tidal elevation from Equation (4.7). For $\alpha = 1$, the total elevation is comprised of the sum of the tidal and residual elevations, which corresponds to the observed water level. For tidal boundaries 1,3,4, and 5 in Table 4.17, the corresponding tidal signals reconstructed from the harmonic constants are used for all boundary cells. For tidal boundary 2, the following linear spatial interpolation procedure is employed to specify $\eta^m_{i,j}$ from boundary signals I_1=2 and I_2=3, in which JB, IL, and IU are as given in Table 4.17.

$$\eta^m_{i,j} = f_{I_1} ht_{I_1}(m\Delta t_E) + f_{I_2} ht_{I_2}(m\Delta t_E) = \eta_a(t) \tag{4.9}$$

$j = JB$
$i = IL, IU$

with $f_{I_1} = \dfrac{(IU - i)}{(IU - IL)}$, $f_{I_2} = \dfrac{(i - IL)}{(IU - IL)}$

where

$ht_{I_1}(m\Delta t_E)$ ≡ Tidal elevation boundary signal at (IL, JB) at time $m\Delta t_E$,
$ht_{I_2}(m\Delta t_E)$ ≡ Tidal elevation boundary signal at (IU, JB) at time $m\Delta t_E$, and
$\eta^m_{i,j}$ ≡ Water surface elevation at time $m\Delta t_E$ at (i, j).

Hourly residual water levels based upon local standard time are specified at The Battery, NY, (851-8750) and at Montauk, NY (851-0560). Water level residuals at The Battery, NY are applied to the reconstructed levels for boundary signal BD5. The Montauk, NY, water level residuals are applied to reconstructed levels for boundary signals BD2, BD3, and BD4. A temporal interpolation is employed to determine the water level residuals at each external-mode time step. For salinity and temperature boundary specification, assume that n_i observed CTD profiles are available at time t_i, i = 0,1, ..., NF, where NF represents the number of observational times.

Table 4.17. Water Surface Elevation Open Boundary Specification

Boundary Description	Type	Grid Location	Tidal Signals	Residual Tide Station
The Battery, NY	S	(16,2)	BD1	851-8750
Montauk Pt., NY	I	(83-92,20)	BD2,BD3	851-0560
Block Island South, RI	S	(92,19-23)	BD3	851-0560
Block Island North, RI	S	(97,29-36)	BD4	851-0560
Spuyten Duyvil, NY	S	(10,9)	BD5	851-8750

S = Specified using tidal signal in column 5
I = Interpolated as a linear function of distance using tidal signals BD2 and BD3

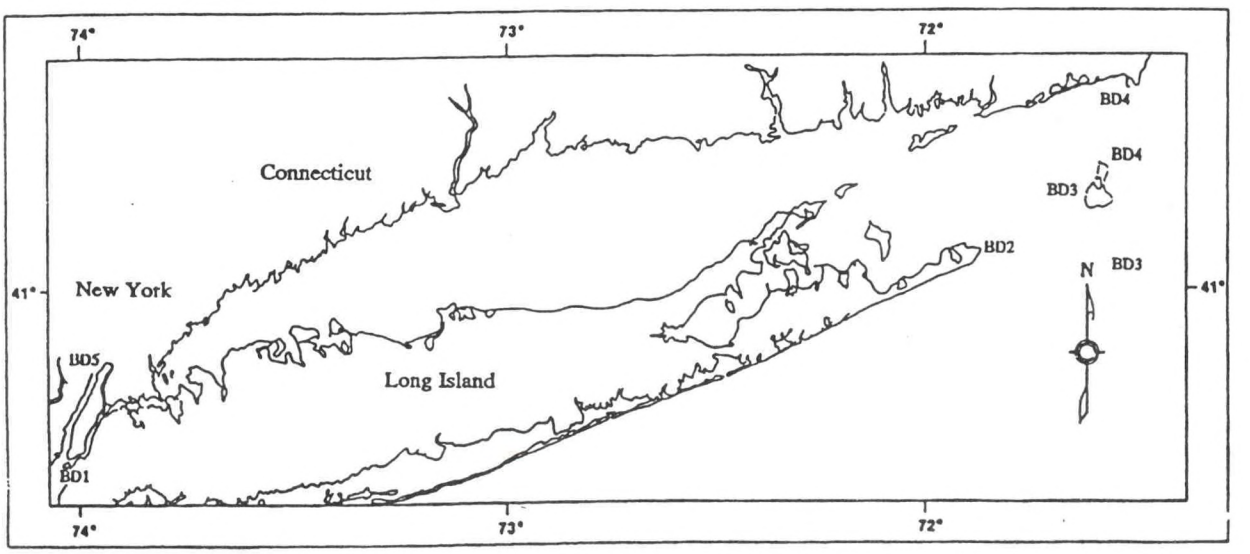

Figure 4.3. Water Surface Elevation Boundary Signals

For each open boundary signal, *nb*, *nb* = *1*, ..., *nbound*, where *nbound* represents the total number of open boundary signals, the complete specification of the salinity and temperature at time $t \in (t_{i-1}, t_i)$ at model level k is determined using the following relationship.

$$T_{nb,k}(t) = T_S(t) + \Delta T_k(t) \quad , \quad S_{nb,k}(t) = S_S(t) + \Delta S_k(t) \quad ,$$

$$T_S(t) = \bar{T}_{nb}(t) + T_{a_{nb}}(t) \cos\left(st + (V_o + u)_T - \phi_{T_{nb}}(t)\right) \quad , \text{ and} \tag{4.10}$$

$$S_S(t) = \bar{S}_{nb}(t) + S_{a_{nb}}(t) \cos\left(a_{M_2} t + (V_o + u)_S - \phi_{S_{nb}}(t)\right) \quad .$$

where all terms are analogous to those in Equation (4.4). The empirical climatological form presented above is used to compute salinity and temperature values at each internal mode time step on the eastern Block Island Sound open ocean boundary. On the western open boundaries at The Battery and Spuyten Duyvil, NY, time series at irregular daily intervals of near surface and near bottom salinity and temperature supplied by EPA were used. All boundary values are prescribed as boundary conditions only on inflow. For each boundary signal, the surface and bottom values are specified as in Tables 4.18 and 4.19 for salinity and as in Tables 4.20 and 4.21 for temperature, respectively. Note that salinity and temperature are specified at the same horizontal grid locations as water surface elevations as shown in Table 4.17. In May - July 1990, Wei (1992) noted that, as far as salinity and temperature fields were concerned, no differences occurred between simulations using the above empirical climatological form and those using CT data based boundary conditions on the Block Island Sound open ocean boundary BD1 and BD5 *(S,T)* time series.

Table 4.18. Salinity Boundary Conditions at The Battery, NY and Spuyten Duyvil, NY

	The Battery, NY (BD1)			Spuyten Duyvil, NY (BD5)		
Date	Surface (psu)	Bottom (psu)	Difference (psu)	Surface (psu)	Bottom (psu)	Difference (psu)
1 Apr 88	20	21.8	1.8	2.3	10.2	7.9
1 May	22.5	24.0	1.5	3.1	10.7	7.6
1 June	22.6	23.2	0.6	6.5	13.4	0.9
1 July	25.2	26.5	1.3	8.2	14.7	6.5
1 Aug	25.0	25.0	0.0	8.0	14.6	6.6
1 Sep	23.9	25.2	1.3	5.7	12.8	7.1
1 Oct	23.7	25.0	1.3	8.2	14.8	6.6
1 Nov	23.8	25.0	1.2	4.8	12.1	7.3
1 Dec 88	20.1	21.6	1.5	3.0	10.7	7.7
1 Jan 89	22.5	23.7	1.2	5.0	12.3	7.3
1 Feb	22.6	23.3	0.7	5.6	12.7	7.1
1 Mar	19.9	22.8	2.9	6.2	13.2	7.0
1 Apr	17.1	21.0	2.9	2.0	9.0	7.0
1 May	21.3	22.7	1.4	4.6	12.0	7.4
1 June	21.8	22.7	0.9	6.1	13.1	7.0
1 July	23.3	23.3	0.0	5.9	12.4	6.5
1 Aug	24.6	24.6	0.0	12.3	15.2	2.9
1 Sep	24.7	24.8	0.1	11.6	17.4	5.8
1 Oct 89	23.5	23.5	0.0	7.8	14.7	6.9

Note : Mean amplitude at BD1 and BD5 equal to 0.4 psu.
Mean phases at BD1 and BD5 equal to 238° and 261°, respectively.

Table 4.19. Salinity Boundary Conditions at the Open Ocean

	Montauk Point N.Y. (BD2)			Block Island South (BD3)			Block Island North (BD4)		
Date	Mean (psu)	Station	Julian Date	Mean (psu)	Station	Julian Date	Mean (psu)	Station	Julian Date
1 Apr 88	30.4	O1	96	30.4	P2	95	31.0	P2	95
1 May	31.0	P2	133	31.0	P2	133	31.0	P2	133
1 June	31.0	P2	139	31.0	P2	139	31.0	P2	139
1 July	31.0	P2	139	31.0	P2	139	31.0	P2	139
1 Aug	31.0	P2	215	31.0	P2	215	31.0	P2	215
1 Sep	30.7	O1	250	31.4	P1	250	32.0	P3	250
1 Oct	30.7	O1	250	31.4	P1	250	32.0	P3	250
1 Nov	32.0	P3	292	32.0	P3	292	32.0	P3	292
1 Dec 88	32.0	P3	292	32.0	P3	292	32.0	P3	292
1 Jan 89	32.0	N3	23	32.0	N3	23	32.0	N3	23
1 Feb	32.0	N3	37	32.0	N3	37	32.0	N3	37
1 Mar	32.0	N3	68	32.0	N3	68	32.0	N3	68
1 Apr	32.0	N3	80	32.0	N3	80	32.0	N3	80
1 May	32.0	N3	128	32.0	N3	128	32.0	N3	128
1 June	30.0	N3	156	30.0	N3	156	30.0	N3	156
1 July	30.0	N3	186	30.0	N3	186	30.0	N3	186
1 Aug	30.0	N3	219	30.0	N3	219	30.0	N3	219
1 Sep	30.0	N3	248	30.0	N3	248	30.0	N3	248
1 Oct 89	30.0	N3	248	30.0	N3	248	30.0	N3	248

Note: Mean Amplitude at BD2, BD3, and BD4 equal 0.4 psu
Phase at BD2 (214° - 219°)
Phase at BD3 (218° - 219°)
Phase at BD4 (218° - 219°)

Table 4.20. Temperature Boundary Conditions at The Battery, NY and Spuyten Duyvil, NY

	The Battery, NY (BD1)			Spuyten Duyvil, NY (BD5)		
Date	Surface (°C)	Bottom (°C)	Difference (°C)	Surface (°C)	Bottom (°C)	Difference (°C)
1 Apr 88	8.6	8.6	0.0	12.4	11.1	1.3
1 May	10.6	9.6	1.0	14.4	13.1	1.3
1 June	17.1	16.2	0.9	20.9	19.6	1.3
1 July	18.4	18.0	0.4	22.2	20.9	1.3
1 Aug	23.6	23.2	0.4	27.4	26.1	1.3
1 Sep	22.7	22.3	0.4	26.5	25.2	1.3
1 Oct	19.4	19.0	0.4	23.2	21.9	1.3
1 Nov	12.8	12.8	0.0	16.6	15.3	1.3
1 Dec 88	11.1	11.1	0.0	14.9	13.6	1.3
1 Jan 89	5.0	5.0	0.0	8.8	7.5	1.3
1 Feb	5.6	5.6	0.0	9.4	8.1	1.3
1 Mar	3.3	3.3	0.0	7.1	5.8	1.3
1 Apr	7.2	7.2	0.0	11.0	9.7	1.3
1 May	11.7	11.3	0.4	15.5	14.2	1.3
1 June	17.2	16.8	0.6	21.0	19.7	1.3
1 July	21.9	21.2	0.7	23.9	22.6	1.3
1 Aug	22.8	22.3	0.5	24.4	24.0	0.4
1 Sep	23.9	23.5	0.4	27.7	26.4	1.3
1 Oct 89	19.7	19.5	0.2	19.1	19.0	0.1

Note: Mean Amplitude and Phase at BD1 and BD5 equal to 0.3 °C and 0°, respectively

Table 4.21. Temperature Boundary Conditions at the Open Ocean

	Montauk Point N.Y. (BD2)			Block Island South (BD3)			Block Island North (BD4)		
Date	Mean (°C)	Station	Julian Date	Mean (°C)	Station	Julian Date	Mean (°C)	Station	Julian Date
1 Apr 88	4.7	O1	96	4.7	O1	96	4.0	P2	95
1 May	6.2	P2	133	6.2	P2	133	6.2	P2	132
1 June	10.0	P2	139	10.0	P2	139	10.0	P2	132
1 July	14.7	P2	168	14.7	P2	168	14.7	P2	132
1 Aug	17.3	N3	194	17.3	N3	194	17.3	N3	194
1 Sep	19.3	O1	250	19.1	O3	250	18.9	P3	250
1 Oct	17.8	O1	250	17.6	O3	250	17.4	P3	250
1 Nov	12.5	P3	292	12.5	P3	292	12.5	P3	292
1 Dec 88	10.0	M3	354	10.0	M3	354	10.0	M3	354
1 Jan 89	4.0	N3	23	4.0	N3	23	4.0	N3	23
1 Feb	4.5	N3	37	4.5	N3	37	4.5	N3	37
1 Mar	3.0	N3	68	3.0	N3	68	3.0	N3	68
1 Apr	1.0	N3	80	1.0	N3	80	1.0	N3	80
1 May	5.0	N3	128	5.0	N3	128	5.0	N3	128
1 June	13.0	N3	156	13.0	N3	156	13.0	N3	156
1 July	14.9	N3	186	14.9	N3	186	14.9	N3	186
1 Aug	18.8	N3	219	18.8	N3	219	18.8	N3	219
1 Sep	20.0	N3	248	20.0	N3	248	20.0	N3	248
1 Oct 89	17.0	N3	248	17.0	N3	248	17.0	N3	248

The surface boundary conditions, Ω_S, are quite involved since they represent the air-sea interaction. In general, a two flow system must be considered. We first list the boundary conditions in Table 4.22 and then consider the determination of the surface fluxes in detail.

Table 4.22. Surface Boundary (Ω_S) Conditions ($\sigma = 0$)

Equation	Condition
[1,2,3,4,5,6,7]	$\omega = 0$
[2]	$\frac{K_m}{H}\frac{\partial u}{\partial \sigma} = \frac{\rho_a}{\rho_o} C_{SD}\left(u_w^2 + v_w^2\right)^{0.5} u_w \quad , \quad \frac{\partial P_a}{\partial x'} = 0$
[3]	$\frac{K_m}{H}\frac{\partial v}{\partial \sigma} = \frac{\rho_a}{\rho_o} C_{SD}\left(u_w^2 + v_w^2\right)^{0.5} v_w \quad , \quad \frac{\partial P_a}{\partial y'} = 0$
[4]	$\frac{K_H}{H}\frac{\partial T}{\partial \sigma} = q_S \quad \text{or} \quad T(\sigma = 0) = T(t)$
[5]	$\frac{K_H}{H}\frac{\partial S}{\partial \sigma} = (E - P)S$
[6]	$q^2 = B_1^{2/3}\frac{\rho_a}{\rho_o} C_{SD}\left(u_w^2 + v_w^2\right)$
[7]	$q^2 l = 0$

where

(u_w, v_w) ≡ (east , north) wind components at 10m (m/s),
q_S ≡ net surface heat flux (°C-m/s),
$T(t)$ ≡ sea surface temperature time series (°C),
E ≡ evaporation rate (m/s),
P ≡ precipitation rate (m/s),
ρ_a ≡ air density (kg/m^3),
ρ_o ≡ reference water density (kg/m^3),
C_{SD} ≡ surface drag coefficient, and,
B_1 ≡ experimental constant (16.6).

It is necessary to provide near surface (10m) wind and atmospheric pressure anomaly fields, as well as either heat flux or sea surface temperature plus evaporation and precipitation fields. In this study, it is assumed that precipitation and evaporation are equal and that salt flux at the sea surface is zero. Note that $\frac{\partial P_a}{\partial x'} = \frac{\partial P_a}{\partial y'} = 0$; e.g, atmospheric pressure anomalies are considered either zero or uniform in space.

In order to specify the sea surface temperature, consider the surface to be comprised of the same set of patches used previously for developing the complete three-dimensional fields. Assume a set of times, t_i, $i = 0,1,\ldots,NF$, where NF represents the number of times, n_i measurements of sea surface temperature are available at time t_i. These measurements are not taken at any one common time point within the tidal cycle or solar day. Let us assume that time series of sea surface temperature are available for a limited number (perhaps only at opposite open boundaries) of stations so that the mean sea surface temperature, $(\bar{T}_{ij})$, mean amplitude, (AT_{ij}), and mean phase, (ϕ_{ij}), during the solar day at time t_i may be estimated for $j = 1, n_i$. The mean phase, ϕ_{ij}, represents the mean difference of the solar hour angle referenced from midnight from 135 degrees at the time of maximum temperature at time t_i. At each time, t_i, for each of the four corners $(N = 1, \ldots 4)$ of patch L, define the sea surface temperature, $ST_{LN}(t)$, at time, t, in the following manner

$$ST_{LN}(t) = T_{LN}(t) + AT_{LN}(t) \cos\left(st + (V_o + u)_T - \phi_{LN}(t)\right) \tag{4.11}$$

where

$T_{LN}(t)$ ≡ mean daily sea surface temperature at time t,
$AT_{LN}(t)$ ≡ mean daily amplitude at time t,
$\phi_{LN}(t)$ ≡ mean phase at time t,
s ≡ solar hour angular velocity (15°/hr), and
$(V_o + u)_T$ ≡ equilibrium argument for temperature (135°).

Finally, a bilinear spatial interpolation is employed for i ∈ (il_L , iu_L) and j ∈ (jl_L , ju_L) as follows

$$\begin{aligned} SST^L_{ij}(t) &= (1 - \Delta_i)(1 - \Delta_j)\, ST_{L1}(t) + \Delta_i(1 - \Delta_j)\, ST_{L2}(t) \\ &+ \Delta_i\Delta_j\, ST_{L3}(t) + (1 - \Delta_i)\Delta_j\, ST_{L4}(t) \end{aligned} \tag{4.12}$$

where

$SST^L_{ij}(t)$ ≡ sea surface temperature at (i,j) in patch L at time t,
$ST_{LN}(t)$, $N=1,\ldots,4$ are as defined above with $\Delta_i = (i - il_L)/(iu_L - il_L)$, and
$\Delta_j = (j - jl_L)/(ju_L - jl_L)$.

The procedures developed above are employed to determine sea surface temperature at each

internal mode time step. Temporal interpolation is initially performed on the mean surface temperature spatial fields developed at monthly intervals from April 1988 - September 1989 from patch CTD cast definitions (such as given in Table 4.9 for 1 September 1988). The amplitude and phase of the sea surface temperature fluctuations are assumed to be spatially and temporally invariants equal to 0.3 °C and 0 degrees, respectively.

The wind field over the model domain is assumed spatially uniform over one patch, which completely covers the domain. For this patch, *I*, such that $i \in (1, 100), j \in (1, 37)$, a wind signal, *NW*, is specified. This wind signal consists of wind speed (knots) and direction (degrees meteorological convention divided by ten, ° M/10) at hourly intervals. A linear interpolation is used to determine the wind speed and direction at $m\Delta t_E$ as follows

$$W^*_{NW}(m\Delta t_E) = f_1 W^*_{NW}(t) + f_2 W^*_{NW}(t+1) \ni m\Delta t_E \in (t, t+1) \quad (4.13)$$

with $f_1 = t + 1 - m\Delta t_E \quad f_2 = m\Delta t_E - t \qquad k = 1, 2$

where

$W^*_{NW}(m\Delta t_E)$ ≡ wind speed $(k=1)$ or direction $(k=2)$ for signal *NW* at time $(m\Delta t_E)$ and

$W^*_{NW}(t)$ ≡ wind speed $(k=1)$ or direction $(k=2)$ for signal *NW* at time *t* (hourly intervals).

The wind speed is converted from knots to meters per second while direction is multiplied by a factor of 10 to convert to true wind direction. The components in the oceanographic convention (W_x, W_y) for the overland wind speed, $W^1_{NW}(m\Delta t_E)$, are computed using the following relationship.

$$(W_x, W_y) = \left(- W^1_{NW}(m\Delta t_E) \cos\left(W^2_{NW}(m\Delta t_E)\right), - W^1_{NW}(m\Delta t_E) \sin\left(W^2_{NW}(m\Delta t_E)\right)\right). \quad (4.14)$$

The overland wind speed is adjusted to an overwater speed, V_{NW}, using a modified relationship given by Hsu (1988) in the following manner

$$V_{NW} = 1.62 + 1.17 W^1_{NW}(m\Delta t_E) . \quad (4.15)$$

where

V_{NW} ≡ overwater windspeed (m/s) for wind signal *NW* and

$W^1_{NW}(m\Delta t_E)$ ≡ overland windspeed (m/s) for wind signal *NW* at time ($m\Delta t_E$).

The surface drag coefficient, C_{SD}, is determined from the Large and Pond formulation (1981) as follows

$$C_{SD} \times (4106) = \left\{ \begin{array}{ll} 1.2 & V_{NW} < 11 \ (m/s) \\ (0.49 + .065\, V_{NW}) & V_{NW} \geq 11 \ (m/s) \end{array} \right\} .$$

Surface wind stresses in Table 4.22 ([2] and [3]) are computed with respect to model coordinates by setting $(u_w, v_w) = (W_y, W_x)$.

Hourly wind speed (knots) and direction (° M/10) were obtained at La Guardia Airport, New York, and at Bridgeport, Connecticut. Wind speeds represent the observed average one-minute value. All times are given in Local Standard Time. Since data are not available over the entire day at Bridgeport, Connecticut, only the values at La Guardia Airport were used and the assumption was made that these wind values could be used to represent a spatially uniform wind over the entire Long Island - Block Island Sound system. Hourly values were input over the period April 1988 - September 1989 and a temporal linear interpolation was used in obtaining overwater winds at each external-mode time step. The bottom boundary conditions, Ω_b, are first summarized in Table 4.23, followed by a description of the bottom friction mechanics.

Table 4.23. Bottom Boundary (Ω_b) Conditions (σ = -1)

Equation	Condition
[1,2,3,4,5,6,7]	$\omega = 0$
[2]	$\frac{K_m}{H}\frac{\partial u}{\partial \sigma} = C_{BD}\left(u^2 + v^2\right)^{0.5} u\Big\|_{\sigma = -1}$
[3]	$\frac{K_m}{H}\frac{\partial v}{\partial \sigma} = C_{BD}\left(u^2 + v^2\right)^{0.5} v\Big\|_{\sigma = -1}$
[4]	$\frac{K_H}{H}\frac{\partial T}{\partial \sigma} = 0$
[5]	$\frac{K_H}{H}\frac{\partial S}{\partial \sigma} = 0$
[6]	$q^2 = B_1^{2/3} C_{BD}\left(u^2 + v^2\right)\Big\|_{\sigma = -1}$
[7]	$q^2 l = 0$

where

(u, v) ≡ bottom model layer fluid velocity components,
C_{BD} ≡ bottom drag coefficient, and
B_1 ≡ experimental constant (16.6).

The approach employed by Blumberg-Mellor (1987) is to assume

$$C_{BD} = \max\left[\frac{\kappa^2}{\left[\ln(z/z_o)\right]^2}, .0025\right] , \tag{4.17}$$

where $\kappa = 0.4$ is the von Karman constant and z_o is a user specified roughness parameter. The value of z is equal to half the thickness of the bottom model layer. The lower bound on the drag coefficient is set at .0025. In all simulations, a background bottom roughness $z_0 = 2$ cm is used. In the five river systems in the State of Connecticut $z_0 = 4$ cm is specified.

External-Mode

Here we consider the following equation set given in Table 2.2; namely, [1] Continuity Equation, [2] x'-Momentum Equation, and [3] y'-Momentum Equation. All five boundary condition types for each of these three equations are listed in Table 4.24. Note the numbers in square brackets near the left margin in Table 4.24, correspond to equation numbers in Table 2.2.

Note that in the surface boundary condition, C_{SD} is as presented previously in Equation (4.16) for the internal-mode. Atmospheric pressure anomalies are not considered as previously for the internal-mode. Note that the surface wind stress is updated each external-mode time step.

Similarly, in the bottom boundary condition, C_{BD} is as previously presented in Equation (4.17) and u and v are the bottom model layer horizontal velocity components. Note that the bottom friction is updated after each internal-mode time step and is held constant for each external mode time step until the internal-mode is next executed.

4.5. Computational Requirements

The model grid (Figure 4.2), as constructed as a 2 km square rectangular grid with seven vertical levels, affords long term (18 month) simulation on presently available supercomputers (CRAY-YMP2/216). Currently, over 14 hours of CRAY-YMP2/216 Central Processing Unit (CPU) time are required to perform an 18 month simulation. If the horizontal grid resolution were increased to 1 km, a factor of 8 times more CPU time would be required. While an orthogonal grid structure might be used over Long Island Sound, the time step constraint is governed by the smallest cell dimension in the grid. Based upon the present number of grid cells, if one were to use a resolution of 1 km on an orthogonal grid, the cpu time required would be doubled over the present requirements. The East River is included in the present computational grid as a folded "L" shape one-dimensional section and the Harlem River is also included as a one-dimensional section as may be noted in Figure 4.2. In the vicinity of the confluence of the East River and western Long Island Sound, the land/water grid cell boundary no longer corresponds to the geographical shoreline due to the folding and only 3-4 grid cells cover the north-south width of the Sound. Grid resolution horizontally is insufficient in these areas to provide details of the tidal and residual circulations. In the highly energetic, topographically complex region near The Race, the 2km grid resolution is not adequate to locally characterize tidal and residual flows.

Table 4.24. External-Mode Boundary Conditions

Equation	Condition
	Ω_{lc}: Closed Lateral Boundary Condition
[1,2,3]	$\bar{u} = 0$ if $n' = x'$ $\quad \bar{v} = 0$ if $n' = y'$
	Ω_{lf}: Lateral Flow Boundary
[1,2,3]	$\bar{u}_{n'} = \frac{Q}{h\Delta o'} \quad \bar{u}_{o'} = 0$
	Ω_{lo}: Open Lateral Boundary Condition
[1,2,3]	$\eta_{n'} = \eta_a(t)$
[2]	$\frac{\partial(H\bar{u}^2)}{\partial x'} = \frac{\partial(H\overline{uv})}{\partial y'} = 0; \quad \frac{\partial(\bar{u}H)}{\partial x'} = \frac{\partial(\bar{u}H)}{\partial y'} = \frac{\partial(\bar{v}H)}{\partial y'} = 0$
[3]	$\frac{\partial(H\bar{v}^2)}{\partial y'} = \frac{\partial(H\overline{uv})}{\partial x'} = 0; \quad \frac{\partial(\bar{v}H)}{\partial y'} = \frac{\partial(\bar{u}H)}{\partial x'} = \frac{\partial(\bar{v}H)}{\partial x'} = 0$
	Ω_S: Surface Boundary Condition
[2,3]	$(\tau_{Sx}, \tau_{Sy}) = \rho_a C_{SD}\left(u_w^2 + v_w^2\right)^{0.5}(u_w, v_w) \quad , \quad \left(\frac{\partial P_a}{\partial x'}, \frac{\partial P_a}{\partial y'}\right) = (0,0')$
	Ω_b: Bottom Boundary Condition
[2,3]	$(\tau_{bx}, \tau_{by}) = \rho_o C_{BD}\left(u^2 + v^2\right)^{0.5}(u, v)$

In the vertical, seven levels are employed in a sigma coordinate system. The first two layers represent one-tenth of the water column. In the deeper regions of the Sound, the layer thicknesses approach 5-7 meters and may not be adequate to resolve the surface mixed layer and near surface thermal structure. In most of the Sound, the upper level thicknesses are on the order of 2-3 meters and should be adequate to resolve general thermocline structure. Clearly, greater horizontal grid resolution is desirable, albeit at the expense of computer resources. The present grid represents a compromise between efficiency of long-term computation over a large water body (Long Island and Block Island Sounds) and higher spatial resolution.

5. FUTURE MODEL ENHANCEMENTS

The following future model enhancements are considered in turn below: 1) Surface Fluxes, 2) Dynamic Restart, and 3) Dynamical Balances.

5.1. Surface Fluxes

In the present study, sea surface temperature is specified based upon CTD data nearest the surface. Satellite thermal imagery might also be used to further refine local fronts and features within the present scheme. As an alternative, heat fluxes might be computed based upon standard meteorological observations at La Guardia Airport, New York. The objective would be to determine how well the sea surface temperatures based upon heat flux specification matched observations. This approach might be tried for the April - June 1988 period. It would also be of interest in conjunction with this effort to increase the number of vertical levels to about 15 or 20 to study evolution of thermocline structure. It would be anticipated that increasing the number of vertical levels would improve resolution of the thermocline.

In the present study, wind is assumed spatially uniform over the entire Sound system and the atmospheric pressure anomaly is considered zero. For hurricane and Northeasters which pass through or in the near vicinity (within 50km) of any portions of Long Island Sound, this assumption is not valid. For the period April 1988 - September 1989, no hurricanes appear to have influenced the area, although a large storm producing peak surges of approximately 4.0 feet occurred in October 1988. It would be desirable to develop standard wind field and pressure field models for Northeasters and hurricanes as well as a more generalized wind and pressure field description for less severe events. In this manner, surface wind and pressure fields might be developed for the entire eighteen month period. Temporal resolution would increase to hourly increments during storm events and decrease to 6 to 24 hour increments during non-storm periods. With improved spatial and temporal resolution of the wind and atmospheric pressure fields, the model would more accurately simulate the effect of short term events on the overall seasonal and annual cycles.

5.2. Dynamic Restart

Although the present restart procedures preserve the hydrodynamic fields, the resulting restart is not truly dynamic. For example, consider a set of three simulations. Simulation one is started from initialized hydrodynamic fields and is run for 5 time steps. Simulation two is performed in the same manner as simulation one but executed for only 3 time steps. Simulation three is initialized (restarted) with the hydrodynamic fields of simulation two and executed for 2 time steps. For the restart procedure to be truly dynamic, the final hydrodynamic fields of simulation one and three must be identical. Under the present restart procedure, this is not the case. However, the differences are very small and are overcome by forcing within a small number of time steps. For residual circulations, the quasi-dynamic technique of the present study is sufficiently robust.

It would not involve substantial effort to modify the present restart procedure to be truly

dynamic. A truly dynamic restart would be advantageous for studying short term storm events after restarting from longer seasonal periods.

5.3. Dynamical Balances

In order to further understand the simulated complex dynamics at CTD stations, it would be desirable to evaluate separately each term in the finite difference equations for the dynamical balances of momentum, temperature, salinity, and the two turbulence quantities (kinetic energy, macroscale). In this approach, the conservation of the computed solution could be evaluated as well as each individual term in the finite difference conservation statement. The evaluation of the finite difference equations would be confined to station horizontal grid locations over a user specified time step range. In order to demonstrate the procedures, the finite difference equations for the two turbulence quantities would be considered. Dissipation and production of turbulence, and the evaluation of the vertical mixing coefficients could be further investigated under this approach.

6. SUMMARY AND CONCLUSIONS

A three-dimensional circulation model has been documented and applied to Long Island Sound. The governing partial differential equations describing the fluid system have been presented and the finite difference operations developed in operator form. Initial condition procedures and boundary conditions for application to Long Island Sound for tidal and residual circulation have been presented. The detailed application to Long Island Sound in terms of grid development and computational requirements has been developed and recommendations advanced for model enhancement. The following points are emphasized:

1. A three-dimensional hydrodynamic model has been documented and applied to simulate tidal and residual circulations in Long Island Sound.

2. The rectilinear (2 kilometer horizontal spacing with seven vertical levels) computational grid represents a compromise between spatial resolution and computational efficiency dictated by long term (18 month) simulation requirements.

3. In the topographically complex boundary regions of Long Island Sound, near The Race and at the entrance to the East River, the grid resolution is not sufficient to resolve details of the tidal and residual circulations.

4. The computational grid is sufficient to describe residual circulation within the interior regions of Long Island Sound at water quality time and space scales.

5. The computational grid is sufficient to describe tidal water levels and currents within the interior regions of Long Island Sound on tidal atlas time and space scales.

ACKNOWLEDGEMENTS

This study was initiated under the supervision of Dr. Henry R. Frey, former Chief, Coastal and Estuarine Oceanography Branch. His guidance and direction to the key elements were essential in keeping the modeling effort focused and in the preparation of this report. Drs. Kurt W. Hess and Wayne L. Wilmot provided many fruitful discussions and comments. Dr. Eugene J. Wei provided many valuable insights based upon his application of the model to a 72 day period in May - July 1990. Ms. Karen L. Earwaker was instrumental in coordinating the report and in the preparation of the equations. Mr. Philip H. Richardson assisted in the preparation of the tables. Ms. Melanie Eggers assisted in the preparation and typing of the text. Ms. Brenda W. Via developed the figures.

REFERENCES

Arakawa, A., 1966. Computational design for long-term numerical integration of the equations of fluid motion: two dimensional incompressible flow: Part 1, **Journal of Computational Physics**, 1, 119-143.

Asselin, R., 1972. Frequency filters for time integrations, **Monthly Weather Review**, 100, 487-490.

Blumberg, A.F. and B. Galperin, 1990. On the summer circulation in New York Bight and contiguous estuarine waters, in **Coastal and Estuarine Studies 38: Residual Currents and Long-Term Transport**, R.T. Cheng (editor), Springer-Verlag, New York.

Blumberg, A.F. and D.M. Goodrich, 1990, Modeling of wind-induced destratification in Chesapeake Bay, **Estuaries**, 13(3): 236-249.

Blumberg, A.F. and G.L. Mellor, 1980. A coastal ocean numerical model, in **Mathematical Modelling of Estuarine Physics**, J. Sündermann and K.P. Holz (editors), Springer-Verlag, Berlin.

Blumberg, A.F. and G.L. Mellor, 1987. A description of a three-dimensional ocean circulation model, in **Three Dimensional Coastal Ocean Models**, N.S. Heaps (editor), American Geophysical Union, Washington, DC.

Chow, S.-H., 1971. **A Study of the Wind Field in the Planetary Boundary Layer of a Moving Tropical Cyclone**, Masters Thesis, New York University, Department of Meteorology, New York, NY, pp 58.

Forsch, C. , M. Knudsen, and S.P.L. Sőrensen, 1902. Berichte über die Konstantenbestimmungen zur Aufstellung der Hydrographischen Tabellen. **Kgl. Danske Videnskab. Selskabs, Skifter, Naturvidenskab math., Afdel. X11** 1, 1-151.

Galperin, B., L.H. Kantha, S. Hassid and A. Rossati, 1988. A quasi-equilibrium turbulent energy model for geophysical flows., **J. Atmos. Sci.**, 45, 55-62.

Hamrick, J.M., 1990. The dynamics of long-term mass transport in esturaries, in **Coastal and Estuaries Studies 38: Residual Currents and Long-term Transport**, R.T. Cheng (editor), Springer-Verlag, New York.

Hsu, S.A., 1988. **Coastal Meteorology**, Academic Press, Inc., New York.

Knudsen, M., 1901. **Hydrographical Tables**. G.E.C. Gad, Copenhagen; Williams and Norgate, London.

Large, W.C. and S. Pond, 1981. Open ocean momentum flux measurements in moderate to strong winds. **J. Phys. Oceanography**, 11, 324-326.

Longuet-Higgins, M.S., 1969. On the transport of mass by time-varying ocean currents, **Deep-Sea Research**, 16, 431-477.

Mellor, G.L. and A.F. Blumberg, 1985. Modeling vertical and horizontal diffusivities with the sigma coordinate system, **Monthly Weather Review**, 113, 1379 - 1383.

Mellor, G.L., 1989. **Documentation for A Three-Dimensional, Primitive Equation, Numerical Ocean Model**, Atmospheric and Oceanic Sciences Program, Princeton University.

Mellor, G.L. and T. Yamada, 1982. Development of a turbulence closure model for geophysical fluid problems, **Rev. Geophys. Space Phys.**, 20, 851-875.

Oey, L.Y., G.L Mellor, and R.I. Hires, 1985a. Tidal modeling of the Hudson-Raritan estuary, **Estuarine Coastal Shelf Science**, 20, 511-527.

Oey, L.Y., G.L. Mellor, and R.I. Hires, 1985b. A three dimensional simulation of the Hudson-Raritan estuary: I description of the model and model simulations, **Journal of Physical Oceanography**, 15, 1676-1692.

Oey, L.Y., G.L. Mellor, and R.I. Hires, 1985c. A three dimensional simulation of the Hudson-Raritan estuary: II comparison with observations, **Journal of Physical Oceanography**, 15, 1693-1709.

Patchen, R.C., 1986. Applications of real-time oceanographic data systems, in **Applicatons of Real-Time Oceanographic Circulation Modeling**, B.B. Parker (editor), Marine Technology Society, Washington, D.C., 47-58.

Shureman, P., 1958. Manual of Harmonic Analysis and Prediction of Tides, **Special Publication 98**, U.S. Government Printing Office, Washington, D.C..

Smagorinsky, J., 1963. General circulation experiments with the primitive equations: I the basic experiment, **Monthly Weather Review**, 91, 99 - 164.

Water Resources Data for Connecticut, Water Year 1988, United States Geological Survey, Water Resources Division, Hartford, Connecticut.

Water Resources Data for Connecticut, Water Year 1989, United States Geological Survey, Water Resources Division, Hartford, Connecticut.

Water Resources Data for New York, Water Year 1988 : Volume 1. Eastern New York Excluding Long Island, United States Geological Survey, Water Resources Division, Albany, New York.

Water Resources Data for New York, Water Year 1989 : Volume 1. Eastern New York Excluding Long Island, United States Geological Survey, Water Resources Division, Albany, New York.

Weiss, L., 1989. Personal Communication, United States Geological Survey, Water Resources Division, Hartford, Connecticut.